This article has been accepted for publication in IEEE Transactions on Wireless Communications. This is the author's version which has not been fully edited and content may change prior to final publication. Citation information: DOI 10.1109/TWC.2021.3125924, IEEE Transactions on Wireless Communications

Adaptive Waveform Design for Communication-Enabled Automotive Radars

Ceyhun D. Ozkaptan, *Student Member, IEEE,* Eylem Ekici, *Fellow, IEEE,* Onur Altintas, *Member, IEEE*

***Abstract*—Large-scale deployment of connected vehicles with cooperative sensing technologies increases the demand on the vehicular communication spectrum in 5.9 GHz allocated for the exchange of safety messages. To support the high data rates needed by such applications, the millimeter-wave (mmWave) automotive radar spectrum at 76-81 GHz can be utilized for wideband communication as well. For this purpose, various joint automotive radar-communication (JARC) systems have been proposed in the literature to perform both functions using the same wideband waveform. However, the wideband joint waveforms encounter frequency-selectivity in both radar and communication channels due to multi-path propagation. In this paper, we address the optimal joint waveform design problem to exploit the frequency-selectivity for wideband JARC operations via orthogonal frequency-division multiplexing (OFDM) wherein subcarrier coefficients are designed for optimal power allocation and phase coding. We show that the problem is a non-convex quadratically constrained quadratic programming (QCQP) problem which is known to be NP-hard. Existing approaches to solve QCQP include semidefinite relaxation (SDR) which incurs high time complexity. Instead, we propose approximation methods to solve QCQP more efficiently by leveraging structured matrices and using convex approximations. Finally, we demonstrate the efficacy of the proposed approaches through numerical simulations.**

***Index Terms*—joint radar-communication, automotive radars, adaptive waveform design, nonconvex optimization.**

I. Introduction

As an integral part of Intelligent Transportation Systems (ITS), connected vehicles will promote safer and coordinated transportation through wireless communication and sensing technologies. To enable vehicle-to-everything (V2X) communication with low-latency, a limited amount of bandwidth is allocated at 5.9 GHz spectrum for the exchange of basic safety messages. With the deployment of connected vehicles and the intelligent infrastructure at a larger scale, the V2X spectrum will face a spectrum scarcity problem due to its limited bandwidth. In addition, emerging cooperative sensing and autonomous driving technologies require a large amount of raw sensor and navigation data to be exchanged for improved performance [2], [3]. Hence, the allocated spectrum cannot be used efficiently for broadband applications along with high-priority basic safety messages. A solution to alleviate the scarcity problem and attain higher data rates is to leverage the underutilized millimeter-wave spectrum (mmWave) with larger bandwidths.

Currently, 76-81 GHz mmWave spectrum is allocated for the automotive radar systems with up to 4 GHz of contiguous bandwidth [4]. Higher bandwidth and smaller wavelength in mmWave spectrum enable better radar sensing resolution and accuracy in terms of range, velocity, and angle. The decrease in wavelength also allows smaller size antenna arrays suitable for automotive systems. Since both communication and radar systems compete for spectrum resources to achieve higher data rates and better sensing accuracy, the most direct solution is the spectral isolation of two systems via regulations. Moreover, interference mitigation and avoidance schemes have been studied in the literature to allow co-existence [5].

As an alternative, joint radar and communication systems have been proposed to eliminate mutual interference by using the same waveform for both radar sensing and data transmission [1], [6]–[11]. Employing such a joint system promotes the effective utilization of the spectrum while reducing cost and hardware size. In these studies, radar channels are modeled with *simple point targets* and *white Gaussian noise*. The point target model can be valid for far-field targets with narrowband radar systems. However, wideband radar signals resolve multiple reflectors on vehicles that are modeled as extended targets with multiple scatterers [4], [12]. Similar to frequency-selectivity in multi-tap communication channels, extended targets also act as frequency-selective channels for wideband radar signals. Combined with the interference with non-flat frequency response, the frequency-selectivity can deteriorate the radar detection and estimation performance [13], [14].

Due to their robustness against frequency-selectivity, orthogonal frequency-division multiplexing (OFDM) waveforms are suitable for adaptive joint automotive radar-communication (JARC) systems for simultaneous data transmission and radar sensing. The subcarrier coefficients of OFDM pulses can be optimized accounting for the frequency-selectivity of both radar and communication channels. With an adaptive approach, the radar detection performance can be improved by designing the waveform based on the extended target response and mitigating the effect of interference (i.e., clutter plus noise) in the radar channel. Considering radar and communication requirements, the optimal OFDM waveform generated adaptively for the dual-use transmission system can outperform the single carrier and non-adaptive approaches.

The waveform design problems have been studied in literature for various performance constraints [14]–[18]. In [15], radar code is designed to improve the detection perfor-

This work was supported in part by the NSF under Grant Numbers 1814923, 1955535, and 2030141. A preliminary version of this work has appeared in the proceedings of IEEE INFOCOM 2020 [1].

Ceyhun D. Ozkaptan and Eylem Ekici are with the Department of Electrical and Computer Engineering, The Ohio State University, Columbus, OH 43210 USA (e-mail: ozkaptan.1@osu.edu; ekici.2@osu.edu).

Onur Altintas is with InfoTech Labs, Toyota Motor North America R&D, Mountain View, CA 94043 USA (e-mail: onur.altintas@toyota.com).

1536-1276 (c) 2021 IEEE. Personal use is permitted, but republication/redistribution requires IEEE permission. See https://www.ieee.org/publications/rights/index.html for more information.
Authorized licensed use limited to: The Ohio State University. Downloaded on March 15,2022 at 15:54:36 UTC from IEEE Xplore. Restrictions apply.

This article has been accepted for publication in IEEE Transactions on Wireless Communications. This is the author's version which has not been fully edited and content may change prior to final publication. Citation information: DOI 10.1109/TWC.2021.3125924, IEEE Transactions on Wireless Communications

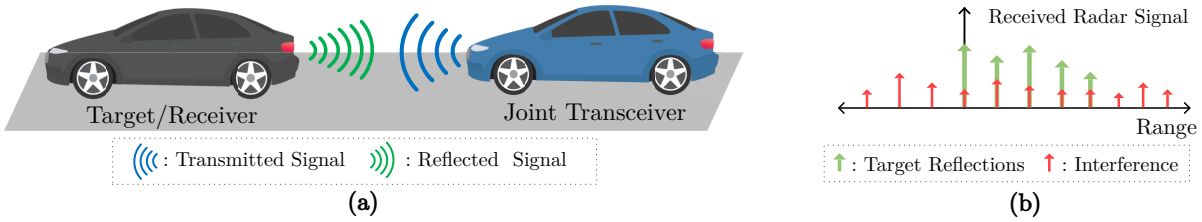

Fig. 1. (a) The operation of the joint communication and radar system on a vehicle (Blue) which receives reflections from the target vehicle (Black) and interference while transmitting data. (b) An illustration of discrete received radar signal.

mance of radar under similarity and unit modulus constraints. In [14], [18], radar waveform is designed to improve the mutual information between the target's impulse response (TIR) and signal that increases the radar's TIR estimation accuracy based on the target's known statistics. In [17], a joint OFDM waveform design problem is studied to increase reflected signal power under interference and autocorrelation shape constraints. However, designed complex weights impede the operation of phase-shift modulation schemes. In these studies, the optimization problems are formulated as non-convex quadratic programming problems and recast as convex semidefinite programming (SDP) problems by dropping *the non-convex rank-one constraint*. While relaxed SDP problems are solved by interior-point algorithms in polynomial time, the time complexity is still high due to the use of higher-dimensional variables. Moreover, the obtained solution is near-optimal with a higher rank due to the relaxation of the rank-one constraint [19]. In this work, our goal is to improve the radar detection performance of the joint OFDM waveform by leveraging previously estimated radar channel, while transmitting communication symbols on the same waveform.

In this work, we consider a JARC transceiver that operates as monostatic radar with colocated transmit and receive antennas. The proposed joint system adaptively optimizes the amplitude and phase values of complex subcarrier weights of transmitted OFDM waveform by leveraging the available information about the radar and communication channels. Since we consider a joint system, the transmitted OFDM waveform also carries communication symbols that are modulated with phase-shift keying (PSK) modulation as illustrated in Fig. 1. Thus, we formulate a joint waveform design problem that improves the radar detection performance while meeting data rate requirements for communication. The proposed waveform design problem is a non-convex quadratically constrained quadratic programming (QCQP) problem and we propose approaches to solve it with *lower time complexity* by exploiting the matrix structures and using convex approximation methods. We also apply the SDP formulation to our problem to compare the time complexity and achieved objective values with the proposed method. Moreover, we propose a generalized approach with lower time complexity. The remainder of this paper is organized as follows: In Section II, we define the system model by formulating the dual-use wideband OFDM signal along with radar and communication channels. In Section III, we formulate the optimization problem to design the OFDM waveform based on given metrics. In Section IV, V, and VI, we propose approximation methods to solve the problem to obtain optimal subcarrier coefficients in real and complex domain with lower time complexity. We present numerical results for the proposed methods in Section VII and conclude our work in Section VIII.

Notations: Boldface lower-case letters denote column vectors as $\mathbf{x}$, boldface upper-case letters denote matrices as $\mathbf{X}$, and plain lower-case letters denote scalars as x. x_i represents the ith element of $\mathbf{x}$. $\mathbb{R}$, $\mathbb{C}$, and $\mathbb{H}$ define the sets of real numbers, complex numbers, and Hermitian matrices, respectively. The transpose, conjugate transpose, trace, and Frobenius norm of $\mathbf{X}$ are denoted by $\mathbf{X}^T$, $\mathbf{X}^\dagger$, $\mathsf{tr}(\mathbf{X})$, and $\|\mathbf{X}\|_F$, respectively. The conjugate, argument, and modulus of a complex number x are given by x^*, $\mathsf{arg}(x)$, and $|x|$, respectively. $\mathsf{Re}(x)$ and $\mathsf{Im}(x)$ return real and imaginary parts of complex number x. Also, $\|\cdot\|$, $\odot$, and $(\cdot)^{\odot}$ represent the Euclidean norm, Hadamard (i.e., element-wise) product and Hadamard power operators. The operator $\mathsf{diag}(\mathbf{X})$ returns a vector with the diagonal elements of square matrix $\mathbf{X}$ and the operator $\mathsf{Diag}(\mathbf{x})$ returns a diagonal square matrix with the elements of $\mathbf{x}$.

II. System Model

A. Signal Model

The dual-use radar and communication system operates at the automotive radar spectrum and transmits a wideband OFDM pulse in each pulse repetition interval (PRI) carrying communication symbols modulated with phase-shift keying (PSK). After the transmission of P pulses that are separated with zeros without cyclic prefix in a coherence processing interval (CPI), the radar receiver processes the reflected pulses by pulse-Doppler processing to generate the range-Doppler image of the illuminated environment [6], [17]. The cyclic prefix is omitted to prevent ambiguities with the correlation-based processing [6], [7]. The transmitted baseband OFDM pulse with N subcarriers denoted as $\tilde{\mathbf{x}} = [\tilde{x}_1 \dots \tilde{x}_N] \in \mathbb{C}^N$ in the time domain and it is generated by precoding symbols with the inverse discrete Fourier transform (IDFT) [20] as

$$\tilde{\mathbf{x}} = \mathbf{W}_N^\dagger \mathbf{x}, \tag{1}$$

where $\mathbf{W}_N \in \mathbb{C}^{N\times N}$ is the unitary DFT matrix for the N-point Fourier Transform and $\mathbf{x} \in \mathbb{C}^N$ is the OFDM signal in the frequency domain. Elements in $\mathbf{x}$ correspond to complex symbols in subcarriers and it is expressed as

$$\mathbf{x} = \mathbf{a} \odot \mathbf{s} = \mathsf{Diag}(\mathbf{s})\mathbf{a}, \tag{2}$$

1536-1276 (c) 2021 IEEE. Personal use is permitted, but republication/redistribution requires IEEE permission. See https://www.ieee.org/publications/rights/index.html for more information.
Authorized licensed use limited to: The Ohio State University. Downloaded on March 15,2022 at 15:54:36 UTC from IEEE Xplore. Restrictions apply.

This article has been accepted for publication in IEEE Transactions on Wireless Communications. This is the author's version which has not been fully edited and content may change prior to final publication. Citation information: DOI 10.1109/TWC.2021.3125924, IEEE Transactions on Wireless Communications

where $\mathbf{s} \in \mathbb{C}^N$ is the modulated symbols comprised of N_p pilot symbols and N_d data symbols. The pilot symbols are included in $\mathbf{s}$ for channel estimation at the communication receiver. Our goal is to design the subcarrier coefficients denoted with $\mathbf{a} \in \mathbb{C}^N$ in (2) for optimal power allocation and phase coding considering both radar and communication performance. The transmitted symbols s is formulated as $\mathbf{s} = \boldsymbol{\mathcal{P}}_\mathrm{p}\mathbf{p} + \boldsymbol{\mathcal{P}}_\mathrm{d}\mathbf{d}$, where $\mathbf{p} = [p_1, p_2, ..., p_{N_\mathrm{p}}]^T$ is pilot symbols, $\mathbf{d} = [d_1, d_2, ..., d_{N_\mathrm{d}}]^T$ is data symbols. $\boldsymbol{\mathcal{P}}_\mathrm{p} \in \{0,1\}^{N \times N_\mathrm{p}}$ and $\boldsymbol{\mathcal{P}}_\mathrm{d} \in \{0,1\}^{N \times N_\mathrm{d}}$ are the permutation matrices for the placement of pilot and data symbols in the frequency domain, respectively. Every column of $\boldsymbol{\mathcal{P}}$ contains only single 1 where the row indices of 1s indicate the indices of the corresponding symbols in $\mathbf{s}$. Thus, the OFDM signal in the frequency domain is formulated as

$$\mathbf{x} = \boldsymbol{\mathcal{P}}_\mathrm{p}\mathbf{x}_\mathrm{p} + \boldsymbol{\mathcal{P}}_\mathrm{d}\mathbf{x}_\mathrm{d},$$

where $\mathbf{x}_\mathrm{p} = \mathbf{a}_\mathrm{p} \odot \mathbf{p}$ and $\mathbf{x}_\mathrm{d} = \mathbf{a}_\mathrm{d} \odot \mathbf{d}$. So, $\mathbf{a}_\mathrm{p}$ and $\mathbf{a}_\mathrm{d}$ are the subcarrier coefficients for pilot and data symbols, where $\mathbf{a}_\mathrm{p} = \boldsymbol{\mathcal{P}}_\mathrm{p}^T\mathbf{a}$ and $\mathbf{a}_\mathrm{d} = \boldsymbol{\mathcal{P}}_\mathrm{d}^T\mathbf{a}$.

B. Radar Channel Model

For the narrowband signal model, the multiple scatterers on a target are not resolved in range, so their response is contained in a single range cell. Thus, the point target assumption is appropriate to model the response of the targets for narrowband radar signals. However, transmitting a signal with a very large bandwidth reduces the size of each range cell (i.e., improves range resolution). As the wideband radar signal resolves each scatterer in range with improved range resolution, the response of the target vehicle *extends* to several range cells [12]. Therefore, the extended targets are modeled with multiple scatterers when wideband transmission is used. Similar to multi-path propagation in a communication channel, the extended target acts like a frequency-selective channel that is represented with a complex finite impulse response (FIR) vector denoted by $\mathbf{g} \in \mathbb{C}^L$, where L is the order of target impulse response (TIR, i.e., target's radar signature) whose total reflecting power scales based on target's distance.

In practice, the TIR is initially unknown but it can be estimated with minimum mean squared error (MMSE) estimator [21] by using prior information about its mean $\boldsymbol{\mu}_\mathrm{g}$ and covariance $\boldsymbol{\Sigma}_g$. If no prior information is available, it can be estimated with a maximum likelihood estimator (MLE) [16]. Since the target's relative velocity and the total duration of OFDM pulses are relatively small, we assume that the target is quasi-stationary and its TIR is nonfluctuating over multiple CPIs [9], [13]. Nevertheless, the automotive radar transceiver can still track the changes in the TIR and use the latest estimate for better detection performance as long as the target's response is not masked by clutter plus noise components.

Since the response of the target spans L range cells, $M = N + L - 1$ samples are taken with the receive antenna, which is colocated with the transmit anteanna, in each observation window to decide whether the target is present. In the range cells of interest, where the target is located, the dominant scatterers are from the target. However, clutter return and noise are also received in the same range cells along with the target's response. The received discrete baseband signal is denoted by $\tilde{\mathbf{y}} \in \mathbb{C}^M$ and it is the sum of the reflected signals from the target and the clutter return $\tilde{\mathbf{c}} \in \mathbb{C}^M$ plus thermal noise component $\tilde{\mathbf{n}} \in \mathbb{C}^M$ as defined in [16] in the frequency domain. In matrix form, the received wideband signal $\tilde{\mathbf{y}}$ in the observation window is formulated as

$$\tilde{\mathbf{y}} = \mathbf{T}_\mathrm{g}\tilde{\mathbf{x}} + \tilde{\mathbf{c}} + \tilde{\mathbf{n}},$$

where $\mathbf{T}_\mathrm{g} \in \mathbb{C}^{M \times N}$ is a lower triangular Toeplitz matrix are defined as

$$\mathbf{T}_\mathrm{g} = \begin{bmatrix} g_1 & 0 & \cdots & 0 \\ \vdots & g_1 & \ddots & \vdots \\ g_L & \vdots & \ddots & 0 \\ 0 & g_L & \ddots & g_1 \\ \vdots & \ddots & \ddots & \vdots \\ 0 & \cdots & 0 & g_L \end{bmatrix} \tag{3}$$

for linear convolution of the transmitted OFDM signal with the target's scattering coefficients. We assume that the clutter return $\tilde{\mathbf{c}}$ is modeled as a zero-mean complex wide-sense stationary (WSS) Gaussian process with known covariance $\boldsymbol{\Sigma}_{\tilde{\mathrm{c}}} \in \mathbb{H}^M$, which has a Toeplitz structure. $\tilde{\mathbf{n}} \in \mathbb{C}^M$ is a zero-mean circularly symmetric complex Gaussian noise with covariance $\boldsymbol{\Sigma}_{\tilde{\mathrm{n}}} = \mathbb{E}[\tilde{\mathbf{n}}\tilde{\mathbf{n}}^\dagger] = \sigma_{\tilde{\mathrm{n}}}^2\mathbf{I}_\mathrm{M}$, where $\sigma_{\tilde{\mathrm{n}}}^2$ is the known noise variance. Since the automotive radar spectrum is solely dedicated to vehicles and mmWave signals experience high attenuation, the interference in the radar channel is composed of the complex Gaussian clutter return plus noise components.

After $\tilde{\mathbf{y}}$ is acquired in the observation window, it is processed at the radar receiver with a receive filter denoted with $\tilde{\mathbf{f}} \in \mathbb{C}^M$. The radar signal-to-clutter-plus-noise ratio (SCNR) at the output of the receive processing filter is formulated as

$$\Psi(\tilde{\mathbf{x}}, \tilde{\mathbf{f}}) = \frac{\mathbb{E}\left[\left|\tilde{\mathbf{f}}^\dagger \mathbf{T}_\mathrm{g}\tilde{\mathbf{x}}\right|^2\right]}{\mathbb{E}\left[\left|\tilde{\mathbf{f}}^\dagger \tilde{\mathbf{c}}\right|^2\right] + \mathbb{E}\left[\left|\tilde{\mathbf{f}}^\dagger \tilde{\mathbf{n}}\right|^2\right]}. \tag{4}$$

which determines the detection performance of the radar receiver. Thus, our goal is to maximize the the radar SCNR that can be formalized equivalently for fixed signal as

$$\min_{\tilde{\mathbf{f}} \in \mathbb{C}^M} \quad \tilde{\mathbf{f}}^\dagger\left(\boldsymbol{\Sigma}_{\tilde{\mathrm{c}}} + \boldsymbol{\Sigma}_{\tilde{\mathrm{n}}}\right)\tilde{\mathbf{f}} \;\; \text{s.t.} \;\; \tilde{\mathbf{f}}^\dagger \mathbf{T}_\mathrm{g}\tilde{\mathbf{x}} = 1,$$

This problem is the well-known the minimum variance distortionless response (MVDR) beamformer design problem [22]. Hence, the optimal receive processing $\tilde{\mathbf{f}}^\star$ is obtained in closed-form as $\tilde{\mathbf{f}}^\star = \kappa_f\left(\boldsymbol{\Sigma}_{\tilde{\mathrm{c}}} + \boldsymbol{\Sigma}_{\tilde{\mathrm{n}}}\right)^{-1}\mathbf{T}_\mathrm{g}\tilde{\mathbf{x}}$, where $\kappa_f = (\tilde{\mathbf{x}}^\dagger\mathbf{T}_\mathrm{g}^\dagger(\boldsymbol{\Sigma}_{\tilde{\mathrm{c}}} + \boldsymbol{\Sigma}_{\tilde{\mathrm{n}}})^{-1}\mathbf{T}_\mathrm{g}\tilde{\mathbf{x}})^{-1}$ is the normalization factor which can be omitted since it does not affect the objective function in (4).

By substituting $\tilde{\mathbf{f}}^\star$ into (4), we reformulate the radar SCNR as

$$\Psi(\tilde{\mathbf{x}}) = \tilde{\mathbf{x}}^\dagger\mathbf{T}_\mathrm{g}^\dagger\left(\boldsymbol{\Sigma}_{\tilde{\mathrm{c}}} + \boldsymbol{\Sigma}_{\tilde{\mathrm{n}}}\right)^{-1}\mathbf{T}_\mathrm{g}\tilde{\mathbf{x}} \tag{5}$$

that depends on the transmitted dual-use waveform denoted with $\tilde{\mathbf{x}}$. As defined in [15], the probability of detection is an

1536-1276 (c) 2021 IEEE. Personal use is permitted, but republication/redistribution requires IEEE permission. See https://www.ieee.org/publications/rights/index.html for more information.
Authorized licensed use limited to: The Ohio State University. Downloaded on March 15,2022 at 15:54:36 UTC from IEEE Xplore. Restrictions apply.

This article has been accepted for publication in IEEE Transactions on Wireless Communications. This is the author's version which has not been fully edited and content may change prior to final publication. Citation information: DOI 10.1109/TWC.2021.3125924, IEEE Transactions on Wireless Communications

increasing function of SCNR that is formulated in closed-form as

$$P_{\mathrm{D}} = Q\left(\sqrt{2\Psi(\tilde{\mathbf{x}})}, \sqrt{-2\ln P_{\mathrm{FA}}}\right), \tag{6}$$

where $Q(\cdot,\cdot)$ denotes Marcum Q function and P_{FA} is the desired value of the probability of false-alarm. Therefore, optimizing the subcarrier coefficients $\mathbf{a}$ allows us to improve the radar detection performance of the JARC system. While we focus on designing the waveform for a single target in this work, the proposed design methods can be extended to design multiple waveforms for multiple targets where the joint transceiver employs diverse adaptive waveforms and detectors in a multiplexing manner to track the targets.

Since the transmitted waveform $\tilde{\mathbf{x}}$ is known at the joint radar transceiver, it operates as a cognitive radar that constantly estimates the TIR and the interference (i.e., clutter plus noise) statistics before optimizing the subcarrier coefficients [16], [18]. While the received signal is the sum of the reflections from the target and interference, it is assumed that the reflected signal is stronger than the interference. Thus, the radar receiver can distinguish whether range cells contain a target to estimate the TIR or interference statistics as discussed in [16], [18] and references therein. Once the TIR and interference statistics are attained, this information can be exploited to increase the radar SCNR for improved detection performance and maximum operating range. Thus, our goal is to design the dual-use waveform to improve the radar performance based on available information about the target and radar channel subject to constraints for communication performance and transmit power limitations.

C. Communication Channel Model

In this part, we will formulate the performance metrics for channel estimation error and communication capacity for the joint waveform. The vehicular channel is modeled as a doubly-selective channel due to high mobility and multi-path propagation. But, the time-selectivity due to relative velocities can be ignored considering the maximum Doppler spread is low and the coherence time T_c is longer than symbol time T_s. Also, the channel is assumed to be invariant for a symbol duration and variant for longer periods where the change in the channel can be estimated via pilot symbols in OFDM waveform. By omitting the time-varying property, the FIR of the communication channel is given as $\mathbf{h} = [h_1, h_2, \ldots, h_J]^T$, where each channel tap h_j is modeled as a complex Gaussian with zero-mean and variance of σ_{h}^2.

In matrix form, the received OFDM signal $\mathbf{z}$ is formulated as

$$\mathbf{z} = \mathbf{H}\mathbf{x} + \mathbf{n},$$

where $\mathbf{H} = \mathsf{Diag}(\mathbf{W}_{NJ}\mathbf{h}) = \mathsf{Diag}(H_0, H_1, ..., H_N)$, $\mathbf{W}_{NJ}$ is the N-point DFT matrix with the size of $(N \times J)$, and the additive noise components in $\mathbf{n}$ are independent complex Gaussians with zero-mean and variance of σ_n^2. To decode the received symbols correctly and acquire the CSI, the communication receiver uses pilot symbols to estimate the channel's FIR $\mathbf{h}$ with a linear minimum mean squared error (LMMSE) estimator. The estimated channel FIR denoted with $\hat{\mathbf{h}}$ is sent back to the transmitter. Since PSK modulated symbols are transmitted through subcarriers, the channel capacity with transmitter CSI can be approximated with a saturation limit denoted with C_{sat} as

$$\mathcal{R}(\mathbf{x}_{\mathrm{d}}) = \sum_{i=1}^{N_{\mathrm{d}}} \Delta f \min\left\{\log_2\left(1 + \frac{|x_{\mathrm{d},i}|^2 |\hat{H}_i|^2}{\sigma_n^2}\right), C_{\mathrm{sat}}\right\}, \tag{7}$$

where $\min\{.,.\}$ denotes component-wise minimum operator, and $C_{\mathrm{sat}} = \log_2(K)$ bits/s/Hz for K-PSK modulation as proposed in [23].

To formulate the effective SNR and optimal power allocation between data and pilot subcarriers, we first derive the mean squared error (MSE) of the channel estimator. The received pilot symbols is expressed as $\mathbf{z}_p = \mathbf{H}_{\mathrm{p}}(\mathbf{a}_{\mathrm{p}} \odot \mathbf{p}) + \mathbf{n}_{\mathrm{p}} = \mathbf{H}_{\mathrm{p}}\mathbf{x}_{\mathrm{p}} + \mathbf{n}_{\mathrm{p}}$, where $\mathbf{H}_{\mathrm{p}} = \boldsymbol{\mathcal{P}}_{\mathrm{p}}^T \mathbf{H} \boldsymbol{\mathcal{P}}_{\mathrm{p}}$. This equation can be simplified as $\mathbf{z}_{\mathrm{p}} = \mathbf{x}_{\mathrm{p}} \boldsymbol{\mathcal{P}}_{\mathrm{p}}^T \mathbf{W}_{NJ} \mathbf{h} + \mathbf{n}$, where $\mathbf{x}_{\mathrm{p}} = \mathsf{Diag}(\mathbf{x}_{\mathrm{p}})$ and $\mathbf{z}_{\mathrm{p}}$ is the input of the channel estimator. As derived in [24], the LMMSE channel estimator for the pilot symbols is

$$\hat{\mathbf{h}} = \frac{1}{\sigma_{\mathrm{n}}^2}\left(\boldsymbol{\Sigma}_h^{-1} + \frac{1}{\sigma_{\mathrm{n}}^2}\mathbf{W}_{pJ}^{\dagger}\mathbf{x}_{\mathrm{p}}^{\dagger}\mathbf{x}_{\mathrm{p}}\mathbf{W}_{pJ}\right)^{-1}\mathbf{W}_{pJ}^{\dagger}\mathbf{x}_{\mathrm{p}}^{\dagger}\mathbf{z}_{\mathrm{p}},$$

where $\boldsymbol{\Sigma}_h = \mathbb{E}[\mathbf{h}\mathbf{h}^{\dagger}]$, $\mathbf{W}_{pJ} = \boldsymbol{\mathcal{P}}_{\mathrm{p}}^T \mathbf{W}_{NJ}$ with size of $(N_{\mathrm{p}} \times J)$ and estimation error is $\boldsymbol{e}_h = \mathbf{h} - \hat{\mathbf{h}}$. The MSE of the LMMSE estimator is given in [24] as

$$\xi = \mathsf{tr}\left(\mathbb{E}[\boldsymbol{e}_h \boldsymbol{e}_h^{\dagger}]\right) = \mathsf{tr}\left(\left(\boldsymbol{\Sigma}_h^{-1} + \frac{1}{\sigma_{\mathrm{n}}^2}\mathbf{W}_{pJ}^{\dagger}\mathbf{x}_{\mathrm{p}}^{\dagger}\mathbf{x}_{\mathrm{p}}\mathbf{W}_{pJ}\right)^{-1}\right). \tag{8}$$

As shown in [20], the MSE of the estimator is minimized when $\mathbb{E}[\boldsymbol{e}_h \boldsymbol{e}_h^{\dagger}]$ in (8) is a diagonal matrix. Thus, we allocate equal power to pilot symbols and place them equally spaced in frequency to obtain a diagonal matrix $\mathbb{E}[\boldsymbol{e}_h \boldsymbol{e}_h^{\dagger}]$. Then, the MSE due to estimation error becomes

$$\xi = \frac{J\sigma_h^2\sigma_{\mathrm{n}}^2}{\sigma_{\mathrm{n}}^2 + E_{\mathrm{p}}\sigma_h^2}, \tag{9}$$

where $E_{\mathrm{p}} = \mathbf{a}_p^{\dagger}\mathbf{a}_{\mathrm{p}}$ is the total energy of pilot symbols. Imperfect channel estimation at the receiver reduces the effective communication SNR.

Based on [20, (25)], effective SNR is expressed as

$$SNR_{eff} = \frac{E_{\mathrm{d}} J\sigma_h^2 - E_{\mathrm{d}}\xi}{E_{\mathrm{d}}\xi + \sigma_{\mathrm{n}}^2 N_{\mathrm{d}}} \tag{10}$$

in terms of ξ, where $E_{\mathrm{d}} = \mathbf{a}_{\mathrm{d}}^{\dagger}\mathbf{a}_{\mathrm{d}}$ is the total energy of data symbols. After replacing (9) in (10) and solving its derivative equals to zero, optimal power allocation parameter denoted as $\gamma_{\mathrm{opt}} = E_{\mathrm{d}}/(P_{\mathrm{t}}N)$ is derived as

$$\gamma_{\mathrm{opt}} = \left(1 + \sqrt{1 - \frac{(N_{\mathrm{d}} - J)\sigma_{\mathrm{h}}^2 P_{\mathrm{t}} N}{N_{\mathrm{d}} N P_{\mathrm{t}}\sigma_{\mathrm{h}}^2 + N_{\mathrm{d}}\sigma_n^2}}\right)^{-1}, \tag{11}$$

where P_{t} is the total signal power equal to $(E_{\mathrm{d}} + E_{\mathrm{p}})/N$.

With CSI, the transmitter adjusts the total energy allocated to data and pilot subcarriers according to $\gamma_{\mathrm{opt}} = E_{\mathrm{d}}/(P_{\mathrm{t}}N)$ to maximize effective SNR. Since equally powered pilot symbols achieve the minimum MSE, the total pilot energy $E_{\mathrm{p}} = (1 - \gamma_{\mathrm{opt}})P_{\mathrm{t}}N$ is shared equally between pilot subcarriers.

1536-1276 (c) 2021 IEEE. Personal use is permitted, but republication/redistribution requires IEEE permission. See https://www.ieee.org/publications/rights/index.html for more information.
Authorized licensed use limited to: The Ohio State University. Downloaded on March 15,2022 at 15:54:36 UTC from IEEE Xplore. Restrictions apply.

This article has been accepted for publication in IEEE Transactions on Wireless Communications. This is the author's version which has not been fully edited and content may change prior to final publication. Citation information: DOI 10.1109/TWC.2021.3125924, IEEE Transactions on Wireless Communications

III. Problem Formulation

In this section, we focus on designing an optimal joint waveform that maximizes the received radar SCNR. Thus, we aim to maximize (4) in terms of $\tilde{\mathbf{x}}$ while preserving the PSK modulation and meeting the requirements of the communication system. For communication, we want to minimize the MSE in channel estimation and maximize effective SNR with CSI at the transmitter. To maximize the effective communication SNR (10), the JARC system allocates power according to the optimal power allocation γ_{opt} derived in (11).

Moreover, equally powered and spaced pilot symbols achieve the minimum MSE for a given total power as explained in Section II-C. Based on this observation, we choose our permutation matrix $\boldsymbol{\mathcal{P}}_{\text{p}}$ to place pilots periodically in frequency and formulate a constraint as $\mathbf{x}_{\text{p}}^{*} \odot \mathbf{x}_{\text{p}} = E_{\text{p}}/N_{\text{p}}\mathbf{1}_{N_{\text{p}}}$ to force equal power allocation. Also, we limit the maximum transmit power by $\mathbf{x}^{\dagger}\mathbf{x} \leq P_{\text{t}}N$. Regarding the performance metrics of radar and communication, we present the optimization problem for joint OFDM waveform design that maximizes the expected detection performance while complying with communication performance constraints for channel estimation error and capacity. The optimization problem is formulated as

$$\begin{aligned} \max_{\tilde{\mathbf{x}}\in\mathbb{C}^{N}} \quad & \mathbb{E}\left[\tilde{\mathbf{x}}^{\dagger}\mathbf{T}_{\text{g}}^{\dagger}\left(\boldsymbol{\Sigma}_{\tilde{\text{c}}}+\boldsymbol{\Sigma}_{\tilde{\text{n}}}\right)^{-1}\mathbf{T}_{\text{g}}\tilde{\mathbf{x}}\right], \\ \text{s.t.} \quad & \mathsf{C}_1 : \mathcal{R}(\mathbf{x}_{\text{d}}) \geq R_{\min}, \\ & \mathsf{C}_2 : \mathbf{x}_{\text{p}}^{*} \odot \mathbf{x}_{\text{p}} = E_{\text{p}}/N_{\text{p}}\mathbf{1}_{N_{\text{p}}}, \\ & \mathsf{C}_3 : \mathbf{x}^{\dagger}\mathbf{x} \leq P_{\text{t}}N, \\ & \mathsf{C}_4 : \mathbf{l} \preceq \mathbf{x}^{*} \odot \mathbf{x} \preceq \mathbf{u}, \end{aligned} \tag{P1}$$

where $R_{\min}$ in C_1 is the minimum communication rate requirement for (7), C_2 ensures the equal power allocation for pilot symbols for accurate channel estimation, C_3 is the transmit power constraint, and $\mathbf{1}_{N_{\text{p}}}$ is an all-one vector. Also, $\mathbf{l}, \mathbf{u} \in \mathbb{R}_{\geq 0}^{N}$ are the lower and upper power limits on each frequency band to comply with power limitations, respectively.

Notice that the optimization variable $\tilde{\mathbf{x}}$ contains PSK modulated complex symbols $\mathbf{s}$ for communication as shown in (2). Since each symbol in $\mathbf{s}$ has unit-energy with phase modulation, we design complex coefficients in $\mathbf{a}$ by restricting their phase according to the phase of symbols in $\mathbf{s}$. Therefore, we introduce phase constraints to limit the phase of complex subcarrier weights and to allow the communication receiver to demodulate received symbols correctly without the knowledge of $\mathbf{a}$. However, we note that the phase values of subcarrier weights should be lower than the minimum phase difference of the employed PSK modulation (e.g., $< \pi/4$ for quadrature phase-shift keying (QPSK)). Although the use of complex weights enlarges the feasible region compared to real-valued weights, it also reduces the minimum distance between constellations and deteriorates the communication performance. With the phase constraint, we reformulate (P1) as

$$\begin{aligned} \max_{\mathbf{a}\in\mathbb{C}^{N}} \quad & f_{\text{o}}(\mathbf{a}) = \mathbf{a}^{\dagger}\mathbf{Q}\mathbf{a}, \\ \text{s.t.} \quad & \mathsf{C}_1 : \mathcal{R}(\mathbf{a}_{\text{d}}) \geq R_{\min}, \\ & \mathsf{C}_2 : \mathbf{a}_{\text{p}}^{*} \odot \mathbf{a}_{\text{p}} = E_{\text{p}}/N_{\text{p}}\mathbf{1}_{N_{\text{p}}}, \\ & \mathsf{C}_3 : \mathbf{a}^{\dagger}\mathbf{a} \leq P_{\text{t}}N, \\ & \mathsf{C}_4 : \mathbf{l} \preceq \mathbf{a}^{*} \odot \mathbf{a} \preceq \mathbf{u}, \\ & \mathsf{C}_{5.1} : \mathsf{arg}(a_n) \in [-\theta, \theta] \quad \forall n \in \mathcal{I}_{\text{d}}, \\ & \mathsf{C}_{5.2} : \mathsf{arg}(a_n) = 0 \quad \forall n \in \mathcal{I}_{\text{p}}, \end{aligned} \tag{P-O}$$

where θ is the maximum allowed phase offset and $\mathbf{Q} = \mathbf{W}_N\mathbf{T}_{\text{g}}^{\dagger}\left(\boldsymbol{\Sigma}_{\tilde{\text{c}}}+\boldsymbol{\Sigma}_{\tilde{\text{n}}}\right)^{-1}\mathbf{T}_{\text{g}}\mathbf{W}_N^{\dagger} \odot \mathbb{E}[\mathbf{s}\mathbf{s}^{\dagger}]^{*}$. Since pilot subcarriers carry symbols that are fixed and known at the communication receiver, the phase of pilot subcarrier weights are set to zero in $\mathsf{C}_{5.2}$, where $\mathcal{I}_{\text{p}}$ denotes the set of pilot subcarriers indices. Therefore, the phase constraint is used for data symbols whose set of subcarrier indices is denoted with $\mathcal{I}_{\text{d}}$ in $\mathsf{C}_{5.1}$.

For this problem, we consider two cases: the coefficients of $\mathbf{a}$ are designed (i) with *zero-phase constraints* (i.e., $\theta = 0$) in the domain of non-negative real numbers $\mathbb{R}_{\geq 0}^{N}$ as power allocation weights and (ii) with *non-zero phase constraints* (i.e., $\theta \in [0, \pi)$) as phase codes. Moreover, for case (i), we can treat communication symbols in $\mathbf{s}$ as either fixed variables or independent and identically distributed (i.i.d.) random variables with $\mathbb{E}[\mathbf{s}\mathbf{s}^{\dagger}] = \mathbf{I}_N$. While using deterministic $\mathbf{s}$ allows optimizing the actual SCNR, it requires the problem to be solved for every OFDM pulse. On the other hand, random $\mathbf{s}$ assumption lowers the overall computational complexity since the designed coefficient can be used as long as the estimated TIR and communication CSI is available and valid to improve the expected SCNR.

(P-O) is a quadratically constrained quadratic programming (QCQP) problem with a nonlinear capacity constraint in C_1 and phase constraint in C_5. It is a non-convex problem due to the maximization convex quadratic function and non-convex capacity constraint C_1. Thus, obtaining a globally optimal solution is difficult to achieve efficiently. To recast (P-O) as a convex problem, we propose relaxation and approximation methods. Then, we resort to interior-point algorithms to obtain near-optimal solutions in polynomial time as evaluated in [25] for convex second-order cone programming (SOCP) and semidefinite programming (SDP) problems.

IV. Adaptive Joint Waveform Design for $\theta = 0$

A. Semidefinite Relaxation (SDR) Method

In this section, we formulate and solve (P-O) as an SDP problem based on the semidefinite relaxation (SDR) method. The SDRmethod is studied for different NP-hard and non-convex problems in literature [26] to obtain near optimal solutions efficiently. It is also evaluated for Boolean quadratic programming (BQP) and non-convex quadratically constrained quadratic programming (QCQP) problems in [19].

The SDP formulation relies on the fact that quadratic functions of $\mathbf{a}$ are linear in the matrix $\mathbf{A} = \mathbf{a}\mathbf{a}^{\dagger}$ and can be expressed with trace operations, i.e., $\mathbf{a}^{\dagger}\mathbf{Q}\mathbf{a} = \mathsf{tr}\left(\mathbf{Q}\mathbf{A}\right)$. To cast

1536-1276 (c) 2021 IEEE. Personal use is permitted, but republication/redistribution requires IEEE permission. See https://www.ieee.org/publications/rights/index.html for more information.
Authorized licensed use limited to: The Ohio State University. Downloaded on March 15,2022 at 15:54:36 UTC from IEEE Xplore. Restrictions apply.

This article has been accepted for publication in IEEE Transactions on Wireless Communications. This is the author's version which has not been fully edited and content may change prior to final publication. Citation information: DOI 10.1109/TWC.2021.3125924, IEEE Transactions on Wireless Communications

(P-O) as an SDP problem, we change the optimization variable to $\mathbf{A} = \mathbf{a}\mathbf{a}^\dagger$ as

$$\begin{aligned} \max_{\mathbf{A}\in\mathbb{R}^{N\times N}} \quad & \mathsf{tr}\big(\mathbf{Q}\mathbf{A}\big), \\ \text{s.t.} \quad & \mathsf{C}_1 : \mathcal{R}\left(\boldsymbol{\alpha}_{\mathrm{d}}^{\odot 1/2}\right) \geq R_{\min}, \\ & \mathsf{C}_2 : \boldsymbol{\mathcal{P}}_{\mathrm{p}}^T \mathsf{diag}(\mathbf{A}) = E_{\mathrm{p}}/N_{\mathrm{p}}\mathbf{1}_{N_{\mathrm{p}}}, \\ & \mathsf{C}_3 : \mathsf{tr}(\mathbf{A}) \leq P_{\mathrm{t}}N, \quad \mathsf{C}_4 : \mathbf{l} \preceq \mathsf{diag}(\mathbf{A}) \preceq \mathbf{u}, \\ & \mathsf{C}_5 : \mathbf{A} \succeq 0, \qquad\quad \mathsf{C}_6 : \mathsf{rank}(\mathbf{A}) = 1, \end{aligned} \tag{P-SDP}$$

where $\boldsymbol{\alpha}_{\mathrm{d}} = \boldsymbol{\mathcal{P}}_{\mathrm{d}}^T \mathsf{diag}(\mathbf{A})$. While the constraints in C_{1-5} are convex in terms the semidefinite variable $\mathbf{A}$, the rank-one constraint in C_6 is the equivalent of $\mathbf{A} = \mathbf{a}\mathbf{a}^\dagger$ and it is a non-convex constraint. The SDR method is employed by dropping the rank-one constraint to obtain a relaxed convex SDP problem. However, the sum of logarithms constraint C_1 is not an SDP constraint. Thus, we first reformulate C_1 as

$$\mathcal{R}_{\mathrm{gm}}(\boldsymbol{\alpha}_{\mathrm{d}}) = \left(\prod_{i=1}^{N_{\mathrm{d}}} \min\left\{1 + \alpha_{\mathrm{d},i}\lambda_{\mathrm{h},i},\ 2^{C_{\mathrm{sat}}}\right\}\right)^{\frac{1}{N_{\mathrm{d}}}} \geq 2^{\frac{C_{\min}}{N_{\mathrm{d}}}}, \tag{12}$$

where $C_{\min} = R_{\min}/\Delta f$ and $\lambda_{\mathrm{h},i} = |\hat{H}_i|^2/\sigma_n^2$. In fact, $\mathcal{R}_{\mathrm{gm}}$ is the geometric mean formulation of the function in (7). Since (12) is a product of nonnegative affine functions, C_1 of (P-SDP) is recast as a second-order cone constraint similar to formulation in [27, Section 2.3] and converted into an SDP constraint using the Schur complement lemma [27].

Hence, we have a relaxed convex SDP problem without the rank-one constraint as

$$\begin{aligned} \max_{\mathbf{A}\in\mathbb{R}^{N\times N}} \quad & \mathsf{tr}\big(\mathbf{Q}\mathbf{A}\big), \\ \text{s.t.} \quad & \mathsf{C}_1 : \mathcal{R}_{\mathrm{gm}}\left(\boldsymbol{\alpha}_{\mathrm{d}}\right) \geq R_{\min}, \quad \mathsf{C}_2,\ \mathsf{C}_3,\ \mathsf{C}_4,\ \mathsf{C}_5, \end{aligned} \tag{P-SDR}$$

where C_{2-5} from (P-SDP) are not changed. The problem in (P-SDR) is the relaxed convex SDP formulation of the original problem in (P-O) for $\theta = 0$. The convex SDP problems can be solved in polynomial-time using interior-point algorithms [19] to obtain the optimal solution $\mathbf{A}^\star$. If $\mathbf{A}^\star$ is a rank-one matrix, then the optimal weights $\mathbf{a}^\star$ of the original problem can be obtained as $\mathbf{a}^\star = \sqrt{\lambda_{A,1}}\mathbf{v}_{A,1}$ where $\lambda_{A,1}$ and $\mathbf{v}_{A,1}$ denote the largest eigenvalue and corresponding eigenvector of $\mathbf{A}^\star$, respectively.

However, as discussed in [19], the interior-point algorithm always returns a solution with the maximal rank. Although $\mathbf{a}^\star = \sqrt{\lambda_{A,1}}\mathbf{v}_{A,1}$ is the best rank-one approximation of a high-rank solution $\mathbf{A}^\star$, it is a suboptimal and possibly infeasible solution. On the other hand, a feasible solution can be obtained by iteratively solving the SDP with a rank penalty as proposed in [28]. But still, the iterative approach returns a suboptimal solution at the cost of higher computational complexity. With lower computation complexity, we extract a solution as $\mathbf{a}^\star = \mathsf{diag}(\mathbf{A}^\star)^{\odot 1/2}$ that is suboptimal yet a feasible solution regardless of the rank of $\mathbf{A}^\star$.

B. Circulant Approximation (CA) Method

Although the interior-point algorithms solve the convex SDP problem (P-SDR) in polynomial time, the time complexity is still high due to the polynomial increase in the dimension of SDP variables and constraints. As it has been discussed in [19], the SDR approach does not guarantee finding a low-rank result and the interior-point algorithm will return a higher rank solution. Thus, we need more time-efficient approaches.

In this section, we show that quadratic objective function with Toeplitz matrix structures can be formulated as a linear function by resorting to a circulant approximation method and by leveraging the properties of circulant matrices. With this approach, our goal is to reduce the dimension of variables and constraints by exploiting the Toeplitz structures in $\boldsymbol{\mathcal{T}}_{\mathrm{i+n}} = \boldsymbol{\Sigma}_{\tilde{\mathbf{c}}} + \boldsymbol{\Sigma}_{\tilde{\mathbf{n}}}$ and the objective function. For this formulation, we also assume that $\mathbb{E}[\mathbf{s}\mathbf{s}^\dagger] = \mathbf{I}_N$ by treating $\mathbf{s}$ as random with unit-energy symbols.

While Toeplitz matrices are extensively used in signal processing and information theory, its special instance called the circulant matrices provides a more structured form that can be diagonalized by the DFT matrix [29]. Furthermore, it has been shown in [30] that a Toeplitz matrix $\boldsymbol{\mathcal{T}}$ can be approximated into circulant form $\boldsymbol{\mathcal{C}}$ in the sense of minimizing $\|\boldsymbol{\mathcal{T}} - \boldsymbol{\mathcal{C}}\|_F$ and asymptotically equivalent in terms of eigenvalues. Hence, we first employ the circulant approximation method on $\boldsymbol{\mathcal{T}}_{\mathrm{i+n}}$ in which row entries of its circulant approximation $\boldsymbol{\mathcal{C}}_{\mathrm{i+n}}$ are defined as

$$\nu_i = \frac{(M-i)\tau_i + i\tau_{-(M-i)}}{M}, \quad i = 0, \ldots, M-1, \tag{13}$$

where τ_i correspond to ith diagonal element of $\boldsymbol{\mathcal{T}}_{\mathrm{i+n}}$. Using the circulant approximation of $\boldsymbol{\Sigma}_{\tilde{\mathbf{c}}} + \boldsymbol{\Sigma}_{\tilde{\mathbf{n}}}$, we express the objective function of (P-O) as

$$f_{\mathrm{o}}'(\mathbf{a}) = \mathbf{a}^\dagger \mathbf{W}_N \mathbf{T}_{\mathrm{g}}^\dagger \boldsymbol{\mathcal{C}}_{\mathrm{i+n}}^{-1} \mathbf{T}_{\mathrm{g}} \mathbf{W}_N^\dagger \mathbf{a}. \tag{14}$$

Lemma 1. *The inverse of an Hermitian circulant matrix $\boldsymbol{\mathcal{C}}$ is also an Hermitian circulant matrix.*

Proof. Since the circulant matrices are diagonalizable with the DFT, its inverse is expressed as

$$\boldsymbol{\mathcal{C}}^{-1} = \left(\mathbf{W}_M' \mathbf{D}_{\mathcal{C}} \mathbf{W}_M\right)^{-1} = \mathbf{W}_M' \mathbf{D}_{\mathcal{C}}^{-1} \mathbf{W}_M,$$

where $\mathbf{W}_M \in \mathbb{C}^{M\times M}$ is the M-point unitary DFT matrix, and $\mathbf{D}_{\mathcal{C}} \in \mathbb{R}^{M\times M}$ is a diagonal matrix. As $\mathbf{D}_{\mathcal{C}}^{-1}$ is also diagonal matrix, $\boldsymbol{\mathcal{C}}^{-1}$ is an Hermitian circulant matrix. □

Since $\boldsymbol{\mathcal{C}}_{\mathrm{i+n}}^{-1}$ in (14) is a Hermitian circulant matrix based on Lemma 1, the matrix product $\boldsymbol{\mathcal{T}}_{\mathrm{o}} = \mathbf{T}_{\mathrm{g}}^\dagger \boldsymbol{\mathcal{C}}_{\mathrm{i+n}}^{-1} \mathbf{T}_{\mathrm{g}}$ in (14) is also in Toeplitz form. Thus, we can compute the circulant approximation of $\boldsymbol{\mathcal{T}}_{\mathrm{o}}$ denoted with $\boldsymbol{\mathcal{C}}_{\mathrm{o}}$ by using (13). As circulant matrices are diagonalizable with the DFT matrix, the objective function of (P-O) is formulated as

$$f_{\mathrm{o}}''(\mathbf{a}) = \mathbf{a}^\dagger W_N \boldsymbol{\mathcal{C}}_{\mathrm{o}} W_N^\dagger \mathbf{a} = \mathbf{a}^\dagger \boldsymbol{\Lambda}_{\mathrm{o}} \mathbf{a} = \boldsymbol{\lambda}_{\mathrm{o}}^T \boldsymbol{\alpha}, \tag{15}$$

where $\boldsymbol{\Lambda}_{\mathrm{o}} \in \mathbb{R}^{N\times N}$ is a diagonal matrix, $\boldsymbol{\lambda}_{\mathrm{o}} = \mathsf{diag}(\boldsymbol{\Lambda}_{\mathrm{o}})$, and $\boldsymbol{\alpha} = \mathbf{a}^{\odot 2}$. Using (15), we reformulate (P-O) as

$$\begin{aligned} \max_{\boldsymbol{\alpha}\in\mathbb{R}^N} \quad & \boldsymbol{\lambda}_{\mathrm{o}}^T \boldsymbol{\alpha}, \\ \text{s.t.} \quad & \mathsf{C}_1 : \mathcal{R}_{\mathrm{gm}}\left(\boldsymbol{\alpha}_{\mathrm{d}}\right) \geq R_{\min}, \quad \mathsf{C}_2 : \boldsymbol{\alpha}_{\mathrm{p}} = E_{\mathrm{p}}/N_{\mathrm{p}}\mathbf{1}_{N_{\mathrm{p}}}, \\ & \mathsf{C}_3 : \sum_{i=1}^{N} \alpha_i \leq P_{\mathrm{t}}N, \qquad \mathsf{C}_4 : \mathbf{l} \preceq \boldsymbol{\alpha} \preceq \mathbf{u}, \end{aligned} \tag{P-CA}$$

1536-1276 (c) 2021 IEEE. Personal use is permitted, but republication/redistribution requires IEEE permission. See https://www.ieee.org/publications/rights/index.html for more information.
Authorized licensed use limited to: The Ohio State University. Downloaded on March 15,2022 at 15:54:36 UTC from IEEE Xplore. Restrictions apply.

This article has been accepted for publication in IEEE Transactions on Wireless Communications. This is the author's version which has not been fully edited and content may change prior to final publication. Citation information: DOI 10.1109/TWC.2021.3125924, IEEE Transactions on Wireless Communications

where $\boldsymbol{\alpha}_{\mathrm{d}} = \boldsymbol{\mathcal{P}}_{\mathrm{d}}^T \boldsymbol{\alpha}$, and $\boldsymbol{\alpha}_{\mathrm{p}} = \boldsymbol{\mathcal{P}}_{\mathrm{p}}^T \boldsymbol{\alpha}$.

The problem in (P-CA) is a convex SOCP problem with a linear objective function, linear constraints C_{2-4}, and a geometric mean constraint C_1, which can be formulated as a SOCP constraint as explained in Section IV-A. Compared to (P-SDR), the dimension of variables and constraints are reduced and do not increase polynomially due to the linear formulation of the objective function with the circulant approximation. To find the optimal solution $\boldsymbol{\alpha}^\star$ for (P-CA), we also use the interior-point algorithm for SOCP which has better time complexity compared to SDP [31]. Since our original variable $\mathbf{a}$ is a non-negative real vector, we can compute the optimal coefficients as $\mathbf{a}^\star = \sqrt{\boldsymbol{\alpha}^\star}$.

C. Sequential Convex Approximation (SCA) Method

With the CA method, we propose an approximation by exploiting the Toeplitz structured matrices that are formed due to the linear convolution operation and the WSS property of the interference. Compared to the CA, the SDR provides a generalized solution without relying on any assumptions about the structure of matrices. Since SDR is a generalized approach, it can be used to obtain close to optimal power allocation weights for the scenarios with arbitrary interference covariance and deterministic communication symbols $\mathbf{s}$ at the expense of higher time complexity. Although both the CA and SDR approaches find feasible power allocation weights that improve the radar performance, both approaches are restricted in terms of the requirements of matrix structures and semidefinite variables, respectively.

To address the deficiencies of other approaches, we propose a sequential convex approximation (SCA) as a generalized solution that is more computationally efficient than SDR and can handle arbitrary constraints that are affine in terms of subcarrier coefficients $\mathbf{a}$. The problem in (P-O) is a non-convex problem due to the maximization of convex objective function and the non-convex constraint in C_1. As studied in [32], local optimal solutions can be obtained for non-convex problems by solving its locally convex approximations sequentially (i.e., sequential convex programming). Therefore, we resort to the first-order Taylor approximation to linearize the non-convex parts of the problem. The Taylor approximation of the objective function of (P-O) on a point $\mathbf{a}^{(k)}$, which is the solution obtained at kth iteration of SCA, defined by $\bar{f}_{\mathrm{o}}(\mathbf{a})^{(k)} = f_{\mathrm{o}}\left(\mathbf{a}^{(k)}\right) + \nabla f_{\mathrm{o}}\left(\mathbf{a}^{(k)}\right)^T \left(\mathbf{a} - \mathbf{a}^{(k)}\right)$, where $\nabla f_{\mathrm{o}}\left(\mathbf{a}^{(k)}\right) = 2\mathbf{Q}\mathbf{a}^{(k)}$.

While the the communication capacity constraint in (12) is convex in terms of $\boldsymbol{\alpha}_{\mathrm{d}}$, it is a non-convex constraint in $\mathbf{a}_{\mathrm{d}} = \sqrt{\boldsymbol{\alpha}_{\mathrm{d}}}$. Therefore, we linearize the inside of the geometric mean function in (12) by using the Taylor approximation as

$$\bar{\mathcal{R}}_{\mathrm{gm}}^{(k)}(\mathbf{a}_{\mathrm{d}}) = \left(\prod_{i=1}^{N_{\mathrm{d}}} \min\left\{\bar{\rho}\left(a_{\mathrm{d},i}, a_{\mathrm{d},i}^{(k)}\right),\ 2^{C_{\mathrm{sat}}}\right\}\right)^{\frac{1}{N_{\mathrm{d}}}} \geq 2^{\frac{C_{\min}}{N_{\mathrm{d}}}}, \tag{16}$$

where

$$\bar{\rho}\left(a_{\mathrm{d},i}, a_{\mathrm{d},i}^{(k)}\right) = 2a_{\mathrm{d},i}^{(k)} \lambda_{\mathrm{h},i} a_{\mathrm{d},i} - a_{\mathrm{d},i}^{(k)2} \lambda_{\mathrm{h},i} + 1.$$

Algorithm 1: Sequential Convex Approximation

Input: $\mathbf{a}^{(0)}$, η_{sca}: maximum no. of iterations, ϵ_{sca}: stopping tolerance
Output: $\mathbf{a}^\star$: designed subcarrier coefficients

```
for k ← 0 to η_sca do
    a^(k+1) ← Solve (P-SCA-SOCP) for (k)
    if |f(a^(k+1)) − f(a^(k))| / f(a^(k)) < ε_sca then
        a* ← a^(k+1) and break
    end
end
return a*
```

With the Taylor approximation, the capacity constraint (16) is a convex second-order cone constraint as explained in Section IV-A. Based on given Taylor approximations and second-order cone formulations, we formulate the subproblem of SCA as

$$\begin{aligned} \arg\max_{\mathbf{a}\in\mathbb{R}^N} \quad & \bar{f}_{\mathrm{o}}(\mathbf{a})^{(k)}, \\ \text{s.t.} \quad & \mathsf{C}_1 : \bar{\mathcal{R}}_{\mathrm{gm}}^{(k)}(\mathbf{a}_{\mathrm{d}}) \geq 2^{C_{\min}/N_{\mathrm{d}}}, \quad \mathsf{C}_2 : \mathbf{a}_{\mathrm{p}} = \sqrt{E_{\mathrm{p}}/N_{\mathrm{p}}}, \\ & \mathsf{C}_3 : \mathbf{a}^\dagger \mathbf{a} \leq P_{\mathrm{t}} N, \qquad \mathsf{C}_4 : \sqrt{\mathbf{l}} \preceq \mathbf{a} \preceq \sqrt{\mathbf{u}}, \end{aligned} \tag{P-SCA-SOCP}$$

which is a convex SOCP problem which can be solved with interior-point algorithms similar to the SDP problems. Since we resort to local Taylor approximations, we start with a feasible initial point of $\mathbf{a}^{(0)}$ to solve the subproblem in (P-SCA-SOCP). Then, we sequentially solve (P-SCA-SOCP) until convergence based on a stopping criterion described in Algorithm 1 for a maximum number of iterations η_{sca} and tolerance ϵ_{sca} for relative change in objective value.

Although CA and SDR methods can find sub-optimal solutions by relying on numerical approximation and relaxation approaches, they do not provide any guarantee that the obtained solution is a Karush-Kuhn-Tucker (KKT) stationary point of the original problem. While providing exact convergence properties with SCA methods is hard to achieve for non-convex problems, we show that SCA converges to a suboptimal solution in the numerical results. Since we provide inner approximations with the SCA approach, it converges to a KKT stationary point, which can be a local or global optimum, as shown in [32].

D. SCA with Peak-to-Average Power Ratio (PAPR) Constraint

While we propose methods to design optimal power allocation weights, the designed weight can increase the peak-to-average power ratio (PAPR) of the joint OFDM waveform that will cause nonlinear distortions and spectral spreading due to the nonlinearity of power amplifiers at high power [33]. Although various PAPR reduction schemes have been proposed in literature based on clipping, filtering, and coding methods, these schemes incur either additional distortions that increase in the bit error rate (BER) or computational complexity and signaling overhead [33], [34]. Therefore, in this section, we formulate a convex PAPR constraint that can be integrated into the SCA problem to limit the PAPR of the adaptive waveform.

1536-1276 (c) 2021 IEEE. Personal use is permitted, but republication/redistribution requires IEEE permission. See https://www.ieee.org/publications/rights/index.html for more information.
© 2021 IEEE. Personal use is permitted, but republication/redistribution requires IEEE permission. See https://www.ieee.org/publications/rights/index.html for more information.
Authorized licensed use limited to: The Ohio State University. Downloaded on March 15,2022 at 15:54:36 UTC from IEEE Xplore. Restrictions apply.

This article has been accepted for publication in IEEE Transactions on Wireless Communications. This is the author's version which has not been fully edited and content may change prior to final publication. Citation information: DOI 10.1109/TWC.2021.3125924, IEEE Transactions on Wireless Communications

We first define the PAPR constraint for the joint OFDM waveform as

$$\frac{\max\limits_{1\leq n\leq N}|\tilde{x}_n|^2}{1/N\sum_{i=1}^{N}|\tilde{x}_i|^2}\leq\gamma_{\mathrm{papr}},\tag{17}$$

where $\gamma_{\mathrm{papr}}\in\mathbb{R}$ is the desired PAPR limit and $\tilde{x}_n\in\mathbb{C}$ is the nth sample of the OFDM signal in the time domain as defined in (1). The PAPR constraint in (17) is equivalently formulated without the max operator as $|\tilde{x}_n|^2\leq\frac{\gamma_{\mathrm{papr}}}{N}\sum_{i=1}^{N}|\tilde{x}_i|^2$ for all time domain samples where $n\in\{1,...,N\}$. Now, we can formulate the PAPR constraints in quadratic form as

$$\mathbf{a}^{\dagger}\mathsf{Diag}(\mathbf{s}^{\dagger})\mathbf{W}_N\left(\mathbf{\Gamma}_n-\frac{\gamma_{\mathrm{papr}}}{N}\mathbf{I}_N\right)\mathbf{W}_N^{\dagger}\mathsf{Diag}(\mathbf{s})\mathbf{a}\leq 0,\tag{18}$$

for $n\in\{1,...,N\}$ where $\mathbf{\Gamma}_n$ is a sparse matrix with only single one at nth element of its main diagonal to indicate the power of nth time domain sample.

However, the constraints in (18) are non-convex since the matrices of quadratic forms are indefinite. Hence, we first decompose the matrices of quadratic form into a sum of positive semidefinite and negative definite components as $\mathbf{P}_n=\mathbf{P}_n^{+}+\mathbf{P}_n^{-}$, respectively. Since negative definite matrices result in non-convexity, we resort to their convex approximations by linearizing negative definite quadratic components (i.e., $\mathbf{a}^{\dagger}\mathbf{P}_n^{-}\mathbf{a}$) on current iterate of $\mathbf{a}^{(k)}$ as

$$\mathbf{a}^{\dagger}\mathbf{P}_n^{+}\mathbf{a}+2\mathsf{Re}\left(\mathbf{a}^{(k)\dagger}\mathbf{P}_n^{-}\mathbf{a}\right)-\mathbf{a}^{(k)\dagger}\mathbf{P}_n^{-}\mathbf{a}^{(k)}\leq 0,\tag{19}$$

where $\mathbf{P}_n=\mathsf{Diag}(\mathbf{s}^{\dagger})\mathbf{W}_N\left(\mathbf{\Gamma}_n-\frac{\gamma_{\mathrm{papr}}}{N}\mathbf{I}_N\right)\mathbf{W}_N^{\dagger}\mathsf{Diag}(\mathbf{s})$. By incorporating (19) into (P-SCA-SOCP), we ensure that the PAPR is below the predefined limit γ_{papr} while designing the power allocation coefficients (18) with Algorithm 1.

V. Phase Code Design for Dual-Use Waveform

With the methods proposed in Section IV, we solve the problem that is originally defined in the complex domain without the phase constraint C_5 of (P-O). Thus, we design the optimal coefficients in $\mathbf{a}$ as power allocation coefficients without disturbing the phase modulation of complex symbols in $\mathbf{s}$. However, we can extend the feasible region of the problem and increase the achievable SCNR by designing the coefficients of $\mathbf{a}$ in the complex domain. Nevertheless, we limit the phase of complex coefficients to allow demodulation of $\mathbf{s}$ without $\mathbf{a}$.

In this section, we solve the original problem in (P1) with the phase constraint. Without the phase constraint, it is been shown that a complex quadratic problem is NP-hard [35]. In radar literature, similar phase constraints are introduced as *similarity constraint* to design radar codes that are similar to a prefixed sequence. In [15], a method based on the SDR and Gaussian randomization is proposed to design constant modulus radar codes with a similarity constraint. The Gaussian randomization procedure [19] is employed to generate random codes by using the SDR solution as the covariance matrix. However, an excessive number of random samples are required to acquire a near-optimal feasible solution, because randomly generated codes require scaling for feasibility as pointed out in [36].

In our preliminary work in [1], we proposed a two-step approach to design optimal *power allocation* (i.e., modulus) and *phase* (i.e., argument) codes for complex subcarriers coefficients. However, the obtained solutions were suboptimal due to relaxation of the non-convex problem with the non-convex unit modulus constraint. In this work, we improve the two-step approach by introducing an additional step to restrict the feasible region closer to the unit circle without violating convexity. Furthermore, we propose another approach to design optimal phase codes sequentially for each coefficient by leveraging the Hermitian property of matrices.

A. 3-Step Phase Code Design with SDR

In this section, we present a three-step approach for the original problem under phase constraint in (P-O) by exploiting the solution acquired with the SCA, CA methods as the first step. As shown in (P-SDR), the quadratic functions and constraints can be linearized with the SDP formulation. However, the nonlinear phase constraint C_5 in (P-O) prevents linear formulation.

1st Step: In Section IV-B, we show that power coefficients $\boldsymbol{a}$ can be found efficiently in the real domain. In the first step, we assume that $\theta=0$ and find optimal $\boldsymbol{a}^{\star}\in\mathbb{R}_{\geq 0}^{N}$ by solving the problem in the real domain. With $\boldsymbol{a}^{\star}$, we have a feasible power allocation for each subcarrier that satisfies constraints C_{1-4} of (P-O). Hence, we simplify the original problem by changing the domain as

$$\begin{aligned}\max_{\mathbf{u}\in\mathbb{C}^N}\quad & f_{\mathrm{pcd}}(\mathbf{u})=\mathbf{u}^{\dagger}\mathbf{Q}_{\mathrm{a}}\mathbf{u},\\ \text{s.t.}\quad & \mathsf{C}_1:|u_n|=1,\\ & \mathsf{C}_{2.1}:\mathsf{arg}(u_n)\in[-\theta,\theta]\quad\forall n\in\mathcal{I}_{\mathrm{d}},\\ & \mathsf{C}_{2.2}:\mathsf{arg}(u_n)=0\quad\forall n\in\mathcal{I}_{\mathrm{p}},\end{aligned}\tag{P-PCD}$$

to design optimal phase codes. The matrices in the objective function are defined as $\mathbf{Q}_{\mathrm{a}}=\mathsf{Diag}(\mathbf{a}_s^{\dagger})\mathbf{W}_N\mathbf{T}_{\mathrm{g}}^{\dagger}\left(\mathbf{\Sigma}_{\tilde{\mathrm{c}}}+\mathbf{\Sigma}_{\tilde{\mathrm{n}}}\right)^{-1}\mathbf{T}_{\mathrm{g}}\mathbf{W}_N^{\dagger}\mathsf{Diag}(\mathbf{a}_s)$ where $\mathbf{a}_s=\mathbf{a}^{\star}\odot\mathbf{s}$. Notice that (P-PCD) is a quadratic programming problem with a search space restricted to an arc on the unit circle. In other words, we try to find the best possible phase codes for complex subcarrier coefficients to maximize the radar SCNR.

2nd Step: (P-PCD) is a non-convex problem due to the unit modulus constraint C_1 and the maximization of a convex quadratic function. To formulate (P-PCD) as an SDP problem, we first express $\mathsf{C}_{2.1}$ and $\mathsf{C}_{2.2}$ equivalently as

$$\mathsf{C}_2:\mathsf{Re}(\mathbf{u})\succeq\cos(\boldsymbol{\theta}),\tag{20}$$

in the vector form, where $\boldsymbol{\theta}\in\mathbb{R}^N$ is the phase constraint limits for the subcarriers as shown in Fig. 2-(a). Thus, we reformulate (P-PCD) as an SDP problem by introducing an SDP variable $\mathbf{U}=\mathbf{u}\mathbf{u}^{\dagger}$ with a larger feasible region as

$$\begin{aligned}\max_{\mathbf{U},\mathbf{u}}\quad & \mathsf{tr}\left(\mathbf{Q}_{\mathrm{a}}\mathbf{U}\right),\\ \text{s.t.}\quad & \mathsf{C}_1:\mathsf{diag}\left(\mathbf{U}\right)=\mathbf{1}_N,\\ & \mathsf{C}_2:\mathsf{Re}(\mathbf{u})\succeq\cos(\boldsymbol{\theta}),\\ & \mathsf{C}_3:\mathbf{U}=\mathbf{u}\mathbf{u}^{\dagger},\end{aligned}\tag{P-PCD2}$$

1536-1276 (c) 2021 IEEE. Personal use is permitted, but republication/redistribution requires IEEE permission. See https://www.ieee.org/publications/rights/index.html for more information.
© 2021 IEEE. Personal use is permitted, but republication/redistribution requires IEEE permission. See https://www.ieee.org/publications/rights/index.html for more information.
Authorized licensed use limited to: The Ohio State University. Downloaded on March 15,2022 at 15:54:36 UTC from IEEE Xplore. Restrictions apply.

This article has been accepted for publication in IEEE Transactions on Wireless Communications. This is the author's version which has not been fully edited and content may change prior to final publication. Citation information: DOI 10.1109/TWC.2021.3125924, IEEE Transactions on Wireless Communications

While the objective function, C_1, and C_2 in (P-PCD2) are linear, C_3 is a non-convex constraint. Similar to the SDR, we relax C_3 to $\mathbf{U} \succeq \mathbf{u}\mathbf{u}^\dagger$. By using the Schur complement lemma, C_3 is reformulated as an SDP constraint: $\left[\begin{smallmatrix}\mathbf{U} & \mathbf{u}\\ \mathbf{u}^\dagger & 1\end{smallmatrix}\right] \succeq 0$

With the relaxation, a convex feasible region is defined by (20) and the inside of the unit circle as illustrated in Fig. 2(a) with green color. Hence, we have a convex SDP problem that is solved by the interior-point method to obtain the solution $\mathbf{u}^\star$ for (P-PCD2). Then, the solution for (P-PCD) is acquired as $u'_n = u^\star_n/|u^\star_n|$ in which the coefficients are normalized for feasibility.

3rd Step: Nevertheless, the obtained solution is a suboptimal solution for (P-PCD) due to the enlarged feasible region in (P-PCD2). To improve the optimality of the obtained solution, we formulate a problem in the third step with more restricted search space closer to the unit circle based on the obtained first solution $\mathbf{u}'$. The restricted feasible region is a convex circular segment inside the unit circle defined by a secant line expressed as

$$\Omega_n = \mathsf{sin}(\theta)\mathsf{Re}(u_n) - \mathsf{sign}\big(\mathsf{Im}(u'_n)\big)\big(\mathsf{cos}(\theta) - 1\big)\mathsf{Im}(u_n) \succeq \mathsf{sin}(\theta) \quad (21)$$

that is also illustrated in Fig. 2(b) in which two secant lines are drawn for the positive and negative signs of the imaginary part of u'. Notice that the search space for (P-PCD2) is shrunk based on the sign of $\mathsf{Im}(u')$ to search for optimal phase codes closer to the original feasible region in (P-PCD). Finally, we formulate the problem for the third step as

$$\begin{aligned} \max_{\mathbf{U},\mathbf{u}} \quad & \mathsf{tr}\big(\mathbf{Q}_\mathrm{a}\mathbf{U}\big), \\ \text{s.t.} \quad & \mathsf{C}_1 : \mathsf{diag}\big(\mathbf{U}\big) = \mathbf{1}_N, \\ & \mathsf{C}_{2.1} : \Omega_n \succeq \mathsf{sin}(\theta) \quad \forall n \in \mathcal{I}_\mathrm{d}, \\ & \mathsf{C}_{2.2} : u_n = 1 \quad \forall n \in \mathcal{I}_\mathrm{p}, \\ & \mathsf{C}_3 : \left[\begin{smallmatrix}\mathbf{U} & \mathbf{u}\\ \mathbf{u}^\dagger & 1\end{smallmatrix}\right] \succeq 0, \end{aligned} \quad \text{(P-PCD3)}$$

where Ω_n is defined in (21). The problem (P-PCD3) is a convex SDP problem with a restricted feasible region compared to (P-PCD2) and it can be solved by the interior-point algorithm to find the optimal $\mathbf{u}''$. Then, the unit modulus coefficients for (P-PCD) are obtained as $u^\star_n = u''_n/|u''_n|$. Hence, the optimal complex subcarrier coefficients are calculated as $\mathbf{a} = \mathbf{a}^\star \odot \mathbf{u}^\star$, where $\mathbf{a}^\star$ is the real subcarrier coefficient obtained by the CA or SCA algorithm in the first step.

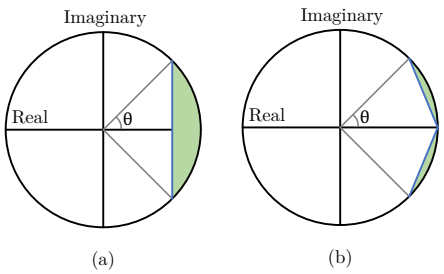

Fig. 2. The feasible regions for the PCD problems.

Algorithm 2: Sequential Phase Code Design

Input: $\mathbf{a}_s$: power allocated symbols, $\mathbf{u}^{(0)}$: initial phase code, ϵ_seq: stopping tolerance,
Output: $\mathbf{u}^\star$: designed phase codes

$k \leftarrow 0$
$\mathbf{Q}_\mathrm{a} \leftarrow \mathsf{Diag}(\mathbf{a}_s^\dagger)\mathbf{W}_N\mathbf{T}_\mathrm{g}^\dagger\big(\mathbf{\Sigma}_{\tilde{\mathbf{c}}} + \mathbf{\Sigma}_{\tilde{\mathbf{n}}}\big)^{-1}\mathbf{T}_\mathrm{g}\mathbf{W}_N^\dagger\mathsf{Diag}(\mathbf{a}_s)$
do
  for $n \leftarrow 1$ ***to*** N **do**
    Compute $\hat{q}_{0n}, \hat{q}_{1n}$ for $\mathbf{Q}_\mathrm{a}$ and $\mathbf{u}^{(k)}$ in (23)
    $\psi^\star_n \leftarrow$ Solve (P7)
    $u^\star_n \leftarrow \mathsf{exp}\left(j\psi^\star_n\right)$
  end
  $\mathbf{u}^{(k+1)} \leftarrow \mathbf{u}^\star$, $k \leftarrow k+1$
while $\left|f_\mathrm{pcd}(\boldsymbol{u}^\star) - f_\mathrm{pcd}\left(\boldsymbol{u}^{(k)}\right)\right| / f_\mathrm{pcd}\left(\boldsymbol{u}^{(k)}\right) < \epsilon_\mathrm{seq}$
return $\boldsymbol{u}^\star$

B. Sequential Phase Code Design

With the 3-step approach, we design optimal phase codes by restricting the search space and then applying to both SCA and SDR methods. However, the time complexity is high since we solve two SDP problems with the interior-point algorithm. In this section, we propose a sequential phase code design method based on [37] to solve quadratic problems with the unit modulus and phase constraint in (P-PCD) with lower time complexity. A quadratic function of $\mathbf{u}$ can be expressed in terms of nth coefficient as

$$\mathbf{u}^\dagger\mathbf{Q}\mathbf{u} + c = \mathsf{Re}\left(u_n \sum_{\substack{m=1\\m\neq n}}^{N} 2q_{mn}u^*_m\right) + \sum_{\substack{k=1\\k\neq n}}^{N}\sum_{\substack{l=1\\l\neq n}}^{N} u^*_l q_{lk} u_k + q_{nn}|u_n|^2 + c, \quad (22)$$

where $\mathbf{Q}$ is a positive semidefinite Hermitian matrix and c is an arbitrary constant. In more compact form, (22) is reformulated as

$$\mathbf{u}^\dagger\mathbf{Q}\mathbf{u} + c = |\hat{q}_{1n}|\,|u_n|\,\mathsf{cos}\big(\phi_{1n} + \psi_n\big) + \hat{q}_{0n} \quad (23)$$

where $\hat{q}_{0n} = \sum_{\substack{k=1\\k\neq n}}^{N}\sum_{\substack{l=1\\l\neq n}}^{N} u^*_l q_{lk}u_k + q_{nn} + c$, $\phi_{1n} = \arg(\hat{q}_{1n})$, $\hat{q}_{1n} = \sum_{\substack{m=1\\m\neq n}}^{N} 2q_{mn}u^*_m$, and $\psi_n = \arg(u_n)$.

By following the formulation in (23) and by using $|u_n| = 1$, we reformulate the quadratic forms in (P-PCD) in terms of nth coefficient's phase ψ_n as

$$\begin{aligned} \underset{\psi_n\in\mathbb{R}}{\arg\max} \quad & |\hat{q}_{1n}|\,\mathsf{cos}\big(\phi_{1n} + \psi_n\big) + \hat{q}_{0n} \\ \text{s.t.} \quad & \mathsf{C}_1 : \psi_n \in [-\theta_n, \theta_n], \end{aligned} \quad \text{(P7)}$$

where θ_n is the phase limit for the nth subcarrier as defined in $\mathsf{C}_{2.1}$ and $\mathsf{C}_{2.2}$ of (P-PCD) for data and pilot symbols, respectively. Since the objective function in (P7) is a cosine function, its maximum is attained at $\psi^\star_n = -\phi_{1n}$, if $-\phi_{1n}$ is in the feasible set of $[-\theta_n, \theta_n]$. Otherwise, the optimal phase code is found at the boundaries of the feasible set that is either $\psi^\star_n = -\theta_n$ or $\psi^\star_n = \theta_n$ based on the attained value of $\mathsf{cos}\left(\phi_{1n} + \psi^\star_n\right)$.

1536-1276 (c) 2021 IEEE. Personal use is permitted, but republication/redistribution requires IEEE permission. See https://www.ieee.org/publications/rights/index.html for more information.
Authorized licensed use limited to: The Ohio State University. Downloaded on March 15,2022 at 15:54:36 UTC from IEEE Xplore. Restrictions apply.

This article has been accepted for publication in IEEE Transactions on Wireless Communications. This is the author's version which has not been fully edited and content may change prior to final publication. Citation information: DOI 10.1109/TWC.2021.3125924, IEEE Transactions on Wireless Communications

This approach is sequentially repeated for all u_n until convergence based on a stopping criteria as described in Algorithm 2. The algorithm stops if the relative change in objective value is lower than given tolerance ϵ_{seq}. Although the phase coefficients in different subcarriers are coupled in the quadratic objective function (22), the sequentially optimizing phase codes in different subcarriers also improves the objective value until it converges to a local or the global maximum depending on the initial starting point [38]. Since the value of the objective function of (P-PCD) is non-decreasing and bounded in each step, the solution will converge to an optimum according to the monotone convergence theorem [39].

VI. PAPR Reduction Routine

In Section IV-D, we introduce a convex PAPR constraint for the SCA method to limit the PAPR of the optimal joint OFDM waveform. But still, the phase code design methods proposed in Section V may increase the PAPR of the waveform. Therefore, in this section, we propose a PAPR reduction routine based on [40] as a complex-valued QCQP problem:

$$\begin{aligned} \min_{\mathbf{u}\in\mathbb{C}^N} \quad & f_{\text{papr}}(\mathbf{u}) = \|\mathbf{u}-\mathbf{u}_{\text{opt}}\|^2, \\ \text{s.t.} \quad & \mathsf{C}_1 : u_n = 1 \quad \forall n \in \mathcal{I}_{\text{p}}, \\ & \mathsf{C}_2 : \mathsf{Re}(u_n) > \cos(\theta_{max}) \quad \forall n \in \mathcal{I}_{\text{d}}, \\ & \mathsf{C}_3 : \mathbf{u}^\dagger \mathbf{R}_n \mathbf{u} \le 0, \\ & \mathsf{C}_4 : |u_n| = 1 \quad \forall n \in \{1,...,N\}, \end{aligned} \tag{P-PAPR}$$

where $\mathbf{u}_{\text{opt}} \in \mathbb{C}^N$ is the designed unit-energy phase codes in the frequency domain, $\mathbf{R}_n = \mathsf{Diag}(\mathbf{a}_s^\dagger)\mathbf{W}_N \left(\mathbf{\Gamma}_n - \frac{\gamma_{\text{papr}}}{N}\mathbf{I}_N\right)\mathbf{W}_N^\dagger \mathsf{Diag}(\mathbf{a}_s)$ in C_3 is the matrix of the quadratic form for the PAPR constraint as explained in Section IV-D where $\mathbf{a}_s = \mathbf{a}^\star \odot \mathbf{s}$. Also, C_1 and C_2 are used to keep pilot symbols fixed and limit the maximum phase shift of data symbols, respectively.

The PAPR reduction problem in (P-PAPR) is used when the PAPR of the designed waveform is above a predefined threshold denoted with γ_{papr} to reduce the PAPR at the expense of deviation from optimized phase codes which can potentially increase the BER and lower the radar SCNR. We reformulate the objective function equivalently as

$$f_{\text{papr}}(\mathbf{u}) = \mathbf{u}^\dagger\mathbf{u} - 2\mathsf{Re}\left(\mathbf{u}_{\text{opt}}^\dagger \mathbf{u}\right). \tag{24}$$

As both the objective function in (24) and C_2 in (P-PAPR) contain linear terms, (P-PAPR) is a non-homogeneous QCQP problem. To recast (P-PAPR) as an SDP problem, we convert non-homogeneous quadratic function in form of $\mathbf{u}^\dagger\mathbf{B}\mathbf{u} + 2\mathbf{b}^\dagger\mathbf{u} = c$ into a homogeneous quadratic function as

$$\begin{bmatrix}\mathbf{u}^\dagger & t\end{bmatrix}\begin{bmatrix}\mathbf{B} & \mathbf{b} \\ \mathbf{b}^\dagger & -c\end{bmatrix}\begin{bmatrix}\mathbf{u} \\ t\end{bmatrix} = 0, \tag{25}$$

where $t \in \mathbb{R}$ is an auxiliary variable that is $t^2 = 1$. Using (25), (P-PAPR) is relaxed as an SDP problem by changing the variable $\mathbf{Y} = \begin{bmatrix}\mathbf{u}^T t\end{bmatrix}^T \begin{bmatrix}\mathbf{u}^T t\end{bmatrix}^* \in \mathbb{C}^{(N+1)\times(N+1)}$ and dropping the rank-one constraint:

$$\begin{aligned} \min_{\mathbf{Y}} \quad & f'_{\text{papr}} = \mathsf{Re}\left(\mathsf{tr}(\mathbf{OY})\right), \\ \text{s.t.} \quad & \mathsf{C}_{1.1} : \mathsf{tr}\left(\begin{bmatrix}\mathbf{0}_N & 1/2\mathbf{e}_n \\ 1/2\mathbf{e}_n^T & -1\end{bmatrix}\mathbf{Y}\right) = 0 \quad \forall n \in \mathcal{I}_{\text{p}}, , \\ & \mathsf{C}_{1.2} : \mathsf{tr}\left(\begin{bmatrix}\mathbf{0}_N & j/2\mathbf{e}_n \\ -j/2\mathbf{e}_n^T & 0\end{bmatrix}\mathbf{Y}\right) = 0 \quad \forall n \in \mathcal{I}_{\text{p}}, \\ & \mathsf{C}_2 : \mathsf{tr}\left(\begin{bmatrix}\mathbf{0}_N & 1/2\mathbf{e}_n \\ 1/2\mathbf{e}_n^T & -\cos(\theta_{max})\end{bmatrix}\mathbf{Y}\right) \ge 0 \quad \forall n \in \mathcal{I}_{\text{d}}, \\ & \mathsf{C}_3 : \mathsf{tr}\left(\ddot{\mathbf{R}}_n\mathbf{Y}\right) \le 0 \ \ \forall n \in \{1,...,N\}, \\ & \mathsf{C}_4 : \mathsf{diag}(\mathbf{Y}) = \mathbf{1}_{N+1}, \quad \mathsf{C}_5 : \mathbf{Y} \succeq 0, \end{aligned} \tag{P-PAPR-SDP}$$

where $\mathbf{O} = \begin{bmatrix}\mathbf{I}_N & -\mathbf{x}_{\text{opt}} \\ -\mathbf{x}_{\text{opt}}^\dagger & 0\end{bmatrix}$, $\ddot{\mathbf{R}}_n = \begin{bmatrix}\mathbf{R}_n & \mathbf{0} \\ \mathbf{0}^T & 0\end{bmatrix}$. Also, $\mathbf{e}_n$ is an indicator vector that contains only a single one at the nth index to obtain the equivalent SDP constraints. The problem in (P-PAPR-SDP) is a convex SDP problem that can be solved with the interior point algorithm to obtain $\mathbf{Y}^\star$. The PAPR-reduced OFDM waveform is computed by $\mathbf{x}^\star = \mathbf{x}'/t'$ where $[\mathbf{x}' \ t]^T = \sqrt{\lambda_{Y,1}}\mathbf{v}_{Y,1}^T$ where $\lambda_{Y,1}$ and $\mathbf{v}_{Y,1}$ denote the largest eigenvalue of $\mathbf{Y}^\star$ and its eigenvector. However, we also note that low values of desired PAPR in C_3 can make the problem infeasible depending on chosen pilot symbols, pilot placements, and phase constraints defined in C_{1-2}.

VII. Numerical Results

In this section, we evaluate the performance of our proposed methods to design the joint OFDM waveform in terms of time complexity and achieved SCNR values. For the time complexity simulations, the number of subcarriers N is the main parameter that affects the performance of proposed approaches. Since the original problem is non-convex, the proposed methods rely on relaxation and approximation approaches to find near-optimal solutions. Thus, we compare the achieved objective values obtained with the baseline performance that is achieved with equal power allocation.

The dual-use system operates in 77 GHz mmWave automotive radar spectrum with 1 GHz bandwidth which achieves the range resolution of $\Delta R = 0.15$ m. The number of pilot subcarriers is $N_{\text{p}} = N/8$ and total transmit power is determined by $P_{\text{t}} = 1$ dB. With given configuration and $N = 128$ subcarriers, we can achieve data rates up to 700 Mbps with unencoded OFDM signal that uses QPSK modulation and guard interval ratio of 2. Moreover, the communication channel is modeled with additive noise variance of $\sigma_n^2 = 1$ and $J = 7$ Rayleigh fading taps with variance $\sigma_h^2 = 1$, which incurs around 7 ns of maximum delay spread. While the communication symbols in $\mathbf{s}$ are assumed to be i.i.d. unit-modulus random variables for the CA approach, they are fixed for other approaches. We consider that the extended radar target is a vehicle modeled with $L = 7$ scatterers resolved in range whose impulse response $\mathbf{g}$ is also randomly generated from $\mathcal{CN}(0, 1)$ distribution. The clutter covariance $\mathbf{\Sigma}_{\tilde{\mathbf{c}}}$ is generated randomly as a positive definite Toeplitz matrix due to its WSS property where diagonal entries are the auto-correlation of a sequence generated from $\mathcal{CN}(0, 1)$ distribution. While the clutter covariance is scaled as $\mathsf{tr}(\mathbf{\Sigma}_{\tilde{\mathbf{c}}}) = 30$ dB, total

1536-1276 (c) 2021 IEEE. Personal use is permitted, but republication/redistribution requires IEEE permission. See https://www.ieee.org/publications/rights/index.html for more information.
Authorized licensed use limited to: The Ohio State University. Downloaded on March 15,2022 at 15:54:36 UTC from IEEE Xplore. Restrictions apply.

This article has been accepted for publication in IEEE Transactions on Wireless Communications. This is the author's version which has not been fully edited and content may change prior to final publication. Citation information: DOI 10.1109/TWC.2021.3125924, IEEE Transactions on Wireless Communications

additive noise covariance for the radar receiver is normalized as $\mathsf{tr}(\mathbf{\Sigma}_{\tilde{\mathrm{n}}}) = 30$ dB.

Based on given parameters, the optimal power allocation parameter γ_{opt} is calculated as in (11) for the transmitter. The minimum capacity requirement R_{min} is determined by the capacity achieved by *the equal power allocated waveform* which is the baseline strategy when no prior information is available. The problems in this work are formulated as convex SDP and SOCP problems which can be solved with interior-point algorithms. Thus, we use the convex optimization toolbox CVX [41] in MATLAB that implements an interior-point algorithm called SDPT3 [42] for SDP and SOCP problems. We run simulations on a PC that is equipped with Intel Core i7-9750H@2.60 GHz processor and 16 GB memory.

A. Achieved SCNR Values

We first evaluate the performance of our proposed approaches in terms of achieved objective values, which are the radar SCNRs for joint OFDM waveform with $N = 128$ subcarriers. The equal power allocated OFDM waveform with real-valued coefficients is used as the baseline non-adaptive approach. Since SDR approach relaxes the rank-one constraint, an upper bound on achieved SCNR is obtained by $\mathsf{tr}\left(\mathbf{Q}\mathbf{A}^{\star}\right)$ where $\mathbf{A}^{\star}$ is the solution of the SDR. As explained in [19], the interior-point algorithm returns higher rank solutions with SDR method which increases the duality gap which is what we observe with the SDR upper bound in Fig. 3.

For the evaluation of achieved SCNR values, the total reflecting power of the target is chosen as the control parameter. While the total clutter plus noise power and the total transmit power are fixed, we use different reflecting powers as $\|\mathbf{g}\|^2 \in \{-3, 0, 3, 6, 9\}$ dB. With given target and clutter parameters, the target-to-clutter-plus-noise ratio is defined as $\mathsf{tr}(\mathbf{T}_{\mathrm{g}}^{\dagger}\mathbf{T}_{\mathrm{g}}) / \left(\mathsf{tr}(\mathbf{\Sigma}_{\tilde{\mathrm{c}}}) + \mathsf{tr}(\mathbf{\Sigma}_{\tilde{\mathrm{n}}})\right) \in \{-2.9, -5.9, -8.9, -11.9, -14.9\}$ dB.

In Fig. 3, the achieved SCNR values are shown for the subcarrier coefficients designed by the SDR, CA, SCA with $\theta = 0$ and, Sequential Phase Code Design (PCD) with $\theta = \{\pi/12, \pi/8, \pi/6\}$. As shown in the figure, the adaptive waveform design approaches achieve around $2\times$ higher SCNR compared to equal power allocation for the given configuration. We also note that the improvement depends on the response of the target, clutter, and communication channel. If the target's response has deep fades over certain frequency bands, the improvement with the adaptive waveform would be greater compared to a frequency-flat response. Moreover, if both communication and the target's response have a similar power spectrum, the adaptive design would achieve even higher SCNR by leveraging the high gain frequency bands with low interference in both radar and communication channels.

Fig. 4 zooms into Fig. 3 with additional results for 2-Step, 3-Step PCD and PAPR reduction approaches. Although the waveform is designed for fixed $\mathbf{s}$ by the SDR approach, it performs slightly worse than both SCA and CA for $\theta = 0$. The reason is that the SDR approach gives suboptimal results due to the removal of the rank-one constraint and the approximation of power allocation coefficients. Since SCA does not require structured matrices, we solve the problem for a given fixed $\mathbf{s}$ with the initial point of equal power allocation and stopping tolerance of $\epsilon_{\mathrm{sca}} = 10^{-4}$. While the SCA is a generalized approach without structured matrix requirement, it achieves a slightly higher SCNR compared to the CA method. However, the improvement with the SCA method in SCNR is limited, so the CA is a better approach for the WSS clutter considering its time complexity. Since an off-the-shelf solver fmincon is available in MATLAB, we also use fmincon as a baseline with default configuration with 10^5 maximum evaluations to solve our problem. While the same initialization with SCA is used, fmincon fails to converge to a better solution compared to SCA.

Furthermore, relaxing the phase constraint with non-zero θ values increases the achieved radar SCNR by expanding the feasible region of the problem in the complex domain as observed in Fig. 4. We observe that 3-Step PCD achieves higher SCNR than 2-Step PCD with an additional third step by restricting the feasible region. Although the search space is restricted for the SDR-based PCD approaches, the interior point algorithm converges to a local maximum. Compared to 3-Step PCD approach, we obtain slightly higher SCNR with Sequential PCD by iteratively optimizing phase codes. Since the search space is restricted to the unit circle, the obtained solution is always feasible and closer to the global optimal of the original problem in (P-PCD). In addition, we evaluate the achieved objective values when the PAPR reduction routine in

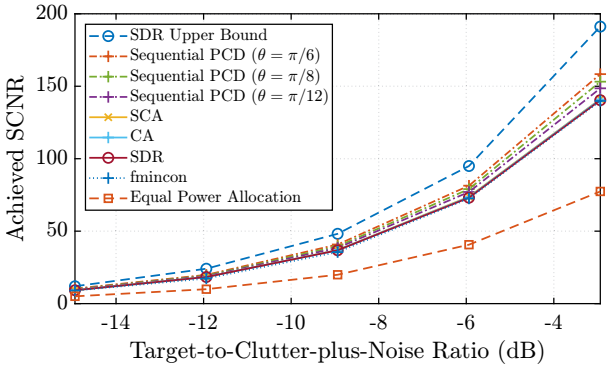

Fig. 3. Obtained SCNR values with proposed waveform design methods

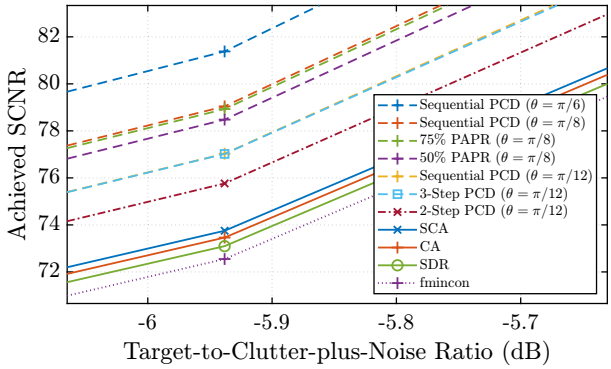

Fig. 4. Zoomed version of Fig. 3 with additional results.

1536-1276 (c) 2021 IEEE. Personal use is permitted, but republication/redistribution requires IEEE permission. See https://www.ieee.org/publications/rights/index.html for more information.
Authorized licensed use limited to: The Ohio State University. Downloaded on March 15,2022 at 15:54:36 UTC from IEEE Xplore. Restrictions apply.

This article has been accepted for publication in IEEE Transactions on Wireless Communications. This is the author's version which has not been fully edited and content may change prior to final publication. Citation information: DOI 10.1109/TWC.2021.3125924, IEEE Transactions on Wireless Communications

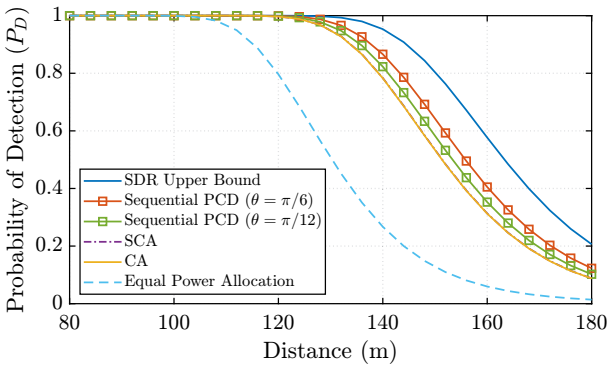

Fig. 5. Achieved probability of detection performance for different distances.

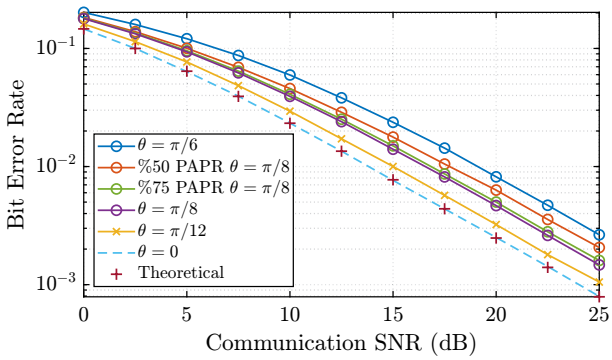

Fig. 7. Achieved bit error rates for different phase and PAPR constraints.

(P-PAPR-SDP) is used with reduction ratios of 50% and 75%. As shown in Fig. 4 for $\theta = \pi/8$, reducing PAPR also lowers the achieved SCNR since the designed phase codes deviate from the optimal phase codes.

To evaluate the achieved detection probabilities, we consider that the target generates a total reflecting power of $\|\mathbf{g}\|^2 = 9$ dB at $R = 80$ m away from the transceiver. As the reflectivity scales with $1/R^4$, we evaluate the achieved detection probabilities at different distances for $P_{\text{FA}} = 10^{-5}$. As shown in Fig. 5, the adaptive approaches increase the detection probability of the extended target which improves the radar's tracking performance and detection distance while meeting the communication constraints.

As seen in the results, the probability of detection performance improves when θ is increased as the feasible search space expands. While increasing θ improves the radar SCNR, it degrades the communication performance by increasing the BER due to reduced distance between symbol constellations as shown in Fig. 7. The theoretical BER is obtained by $1/2\left(1-\sqrt{(E_b/N_0)/(E_b/N_0+1)}\right)$ as derived in [43]. As depicted in the figure, the BER increases with larger θ values. Moreover, the PAPR reduction routine slightly increases the BER due to additional phase perturbation as shown for $\theta = \pi/8$. Since QPSK modulations is used, the increase in BER is low for $\theta < \pi/4$ compared to $\theta = 0$.

B. Time Complexity

For the time complexity evaluations, the randomly generated TIRs are scaled as $\|\mathbf{g}\|^2 = 1$ dB. The total running times are measured to solve (P-O) with the SDR, CA, SCA, and fmincon for $\theta = 0$ and with the PCD approaches for $\theta = \pi/6$. The measured time complexities are shown in Fig. 6 for adaptive power allocation approaches proposed in Section IV for $\theta = 0$ for the different numbers of subcarriers $N \in \{32, 64, 128, 256, 288, 320\}$. As shown, the complexity of SDR and fmincon increases with a higher-order compared to CA and SCA due to semidefinite variables and constraints. In addition, fmincon fails to converge in defined maximum number of evaluations which results in higher time complexity. Considering both higher time complexity and low objective value, fmincon is not a suitable option for the problem.

We can see that the CA approach solves the problem around 16× faster than SDR for 320 subcarriers by leveraging the Toeplitz matrix structures due to linear convolution and the WSS property of clutter. Furthermore, the SCA approach solves the same problem 3× faster than the SDR approach by using sequential approximations. Thus, both of the proposed approaches lower the time complexity for adaptive joint waveform design problem in the real domain.

Fig. 8 shows the measured time complexities for phase code design approaches proposed in Section V for the different numbers of subcarriers $N \in \{32, 64, 128, 256\}$. Since the 3-Step PCD approach includes one more additional step than 2-Step PCD, the measured time for 3-Step PCD is higher

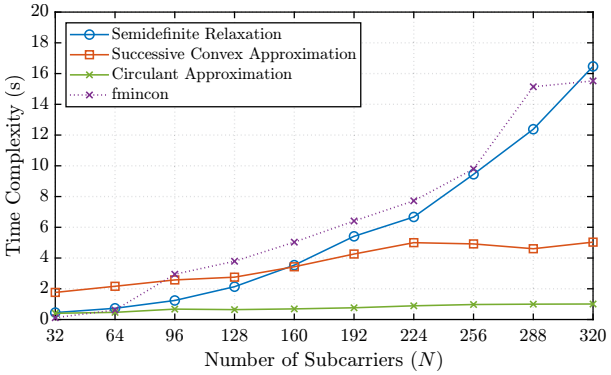

Fig. 6. Time complexity results for proposed methods for $\theta = 0$.

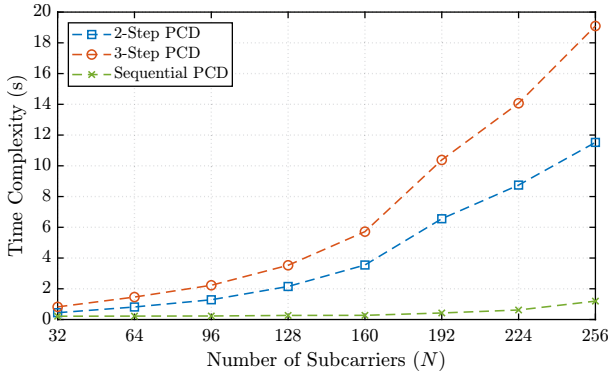

Fig. 8. Time complexity results for proposed PCD methods.

1536-1276 (c) 2021 IEEE. Personal use is permitted, but republication/redistribution requires IEEE permission. See https://www.ieee.org/publications/rights/index.html for more information.
© 2021 IEEE. Personal use is permitted, but republication/redistribution requires IEEE permission. See https://www.ieee.org/publications/rights/index.html for more information.
Authorized licensed use limited to: The Ohio State University. Downloaded on March 15,2022 at 15:54:36 UTC from IEEE Xplore. Restrictions apply.

This article has been accepted for publication in IEEE Transactions on Wireless Communications. This is the author's version which has not been fully edited and content may change prior to final publication. Citation information: DOI 10.1109/TWC.2021.3125924, IEEE Transactions on Wireless Communications

than 2-Step PCD. Due to the use of SDR method in 2-Step and 3-Step PCD, one can observe a similar trend in time complexities compared to the SDR method for $\theta = 0$ in Fig. 6. Also, Sequential PCD approach is run with initial values of ones and tolerance of $\epsilon_{\text{seq}} = 10^{-6}$. As shown in the figure, Sequential PCD method outperforms both 2-Step and 3-Step PCD by around $11\times$ and $19\times$ lower time complexity and higher achieved objective values. Hence, Sequential PCD method is a better method to design optimal phase codes adaptively.

In [44], it is shown that field-programmable gate arrays (FPGAs) can solve interior point algorithms $6.5\times$ faster than general-purpose CPUs. Combined with the hardware implementation, the lower time complexity and affine formulation make the CA, SCA, and Sequential PCD approaches suitable for designing joint waveform adaptively on the orders of milliseconds.

VIII. Conclusion

In this work, we study an adaptive OFDM waveform design problem for JARC systems based on available information about the extended target, and clutter plus noise. First, we investigate the power and subcarrier allocation between data and pilot symbols in the OFDM waveform to minimize the estimation error for the communication channel. Then, we present the design problem to maximize SCNR while maintaining baseline communication capacity achieved with equal power allocated OFDM waveform. We show that the problem is a non-convex QCQP with a sum of logarithms and a phase constraint. For the formulated problem which is a non-convex QCQP, we propose relaxation and approximation approaches to obtain near-optimal solutions with lower time complexity. The numerical results show that both proposed CA and SCA approaches solve the problem in the real domain with higher objective value and low complexity by exploiting the structured matrices and successive approximations. In addition, we further improve the radar SCNR by solving the problem in the complex domain with the proposed PCD approaches. Compared to SDR-based methods, Sequential PCD achieves higher SCNR with lower time complexity by optimizing individual phase codes sequentially where convergence to a local optimum is guaranteed.

References

[1] C. D. Ozkaptan, E. Ekici, and O. Altintas, "Enabling communication via automotive radars: An adaptive joint waveform design approach," in *IEEE INFOCOM 2020 - IEEE Conference on Computer Communications*, July 2020, pp. 1409–1418.

[2] S. Kim, B. Qin, Z. J. Chong, X. Shen, W. Liu, M. H. Ang, E. Frazzoli, and D. Rus, "Multivehicle cooperative driving using cooperative perception: Design and experimental validation," *IEEE Transactions on Intelligent Transportation Systems*, vol. 16, no. 2, pp. 663–680, Apr. 2015.

[3] J. Choi, V. Va, N. Gonzalez-Prelcic, R. Daniels, C. R. Bhat, and R. W. Heath, "Millimeter-wave vehicular communication to support massive automotive sensing," *IEEE Communications Magazine*, vol. 54, no. 12, pp. 160–167, Dec. 2016.

[4] J. Hasch, E. Topak, R. Schnabel, T. Zwick, R. Weigel, and C. Waldschmidt, "Millimeter-wave technology for automotive radar sensors in the 77 GHz frequency band," *IEEE Transactions on Microwave Theory and Techniques*, vol. 60, no. 3, pp. 845–860, Mar. 2012.

[5] K.-W. Huang, M. Bică, U. Mitra, and V. Koivunen, "Radar waveform design in spectrum sharing environment: Coexistence and cognition," in *2015 IEEE Radar Conference (RadarCon)*, May 2015, pp. 1698–1703.

[6] R. F. Tigrek, W. J. A. de Heij, and P. van Genderen, "Multi-carrier radar waveform schemes for range and doppler processing," in *2009 IEEE Radar Conference*, May 2009, pp. 1–5.

[7] C. Sturm and W. Wiesbeck, "Waveform design and signal processing aspects for fusion of wireless communications and radar sensing," *Proceedings of the IEEE*, vol. 99, no. 7, pp. 1236–1259, July 2011.

[8] Y. Han, E. Ekici, H. Kremo, and O. Altintas, "Optimal spectrum utilization in joint automotive radar and communication networks," in *2016 14th International Symposium on Modeling and Optimization in Mobile, Ad Hoc, and Wireless Networks (WiOpt)*, May 2016, pp. 1–8.

[9] P. Kumari, J. Choi, N. González-Prelcic, and R. W. Heath, "IEEE 802.11ad-based radar: An approach to joint vehicular communication-radar system," *IEEE Transactions on Vehicular Technology*, vol. 67, no. 4, pp. 3012–3027, Apr. 2018.

[10] C. D. Ozkaptan, E. Ekici, O. Altintas, and C. Wang, "OFDM pilot-based radar for joint vehicular communication and radar systems," in *2018 IEEE Vehicular Networking Conference (VNC)*, Dec. 2018, pp. 1–8.

[11] D. Ma, N. Shlezinger, T. Huang, Y. Liu, and Y. C. Eldar, "Joint radar-communication strategies for autonomous vehicles: Combining two key automotive technologies," *IEEE Signal Processing Magazine*, vol. 37, no. 4, pp. 85–97, June 2020.

[12] F. Folster, H. Rohling, and U. Lubbert, "An automotive radar network based on 77 GHz FMCW sensors," in *IEEE International Radar Conference, 2005.*, May 2005, pp. 871–876.

[13] M. Richards, W. Holm, and J. Scheer, *Principles of Modern Radar: Basic Principles*, ser. Electromagnetics and Radar. Institution of Engineering and Technology, 2010.

[14] M. Bell, "Information theory and radar waveform design," *IEEE Transactions on Information Theory*, vol. 39, no. 5, pp. 1578–1597, Sept. 1993.

[15] A. De Maio, S. De Nicola, Y. Huang, Z. Luo, and S. Zhang, "Design of phase codes for radar performance optimization with a similarity constraint," *IEEE Transactions on Signal Processing*, vol. 57, no. 2, pp. 610–621, Feb. 2009.

[16] S. Sen and A. Nehorai, "Adaptive OFDM radar for target detection in multipath scenarios," *IEEE Transactions on Signal Processing*, vol. 59, no. 1, pp. 78–90, Oct. 2011.

[17] T. Guo and R. Qiu, "OFDM waveform design compromising spectral nulling, side-lobe suppression and range resolution," in *2014 IEEE Radar Conference*, May 2014, pp. 1424–1429.

[18] C. Shi, F. Wang, M. Sellathurai, J. Zhou, and S. Salous, "Power minimization-based robust OFDM radar waveform design for radar and communication systems in coexistence," *IEEE Transactions on Signal Processing*, vol. 66, no. 5, pp. 1316–1330, Nov. 2018.

[19] Z. Luo, W. Ma, A. M. So, Y. Ye, and S. Zhang, "Semidefinite relaxation of quadratic optimization problems," *IEEE Signal Processing Magazine*, vol. 27, no. 3, pp. 20–34, May 2010.

[20] S. Ohno and G. B. Giannakis, "Capacity maximizing MMSE-optimal pilots for wireless OFDM over frequency-selective block rayleigh-fading channels," *IEEE Transactions on Information Theory*, vol. 50, no. 9, pp. 2138–2145, Sept. 2004.

[21] Y. Yang and R. S. Blum, "MIMO radar waveform design based on mutual information and minimum mean-square error estimation," *IEEE Transactions on Aerospace and Electronic Systems*, vol. 43, no. 1, pp. 330–343, May 2007.

[22] S. Haykin and K. R. Liu, *Handbook on Array Processing and Sensor Networks*. Wiley-IEEE Press, 2010.

[23] W. Guo, S. Wang, and X. Chu, "Capacity expression and power allocation for arbitrary modulation and coding rates," in *2013 IEEE Wireless Communications and Networking Conference (WCNC)*, Apr. 2013, pp. 3294–3299.

[24] S. M. Kay, *Fundamentals of Statistical Signal Processing: Estimation Theory*. Upper Saddle River, NJ, USA: Prentice-Hall, Inc., 1993.

[25] Y. Nesterov and A. Nemirovskii, *Interior-Point Polynomial Algorithms in Convex Programming*. Society for Industrial and Applied Mathematics, 1994.

[26] S. Boyd and L. Vandenberghe, "Semidefinite programming relaxations of non-convex problems in control and combinatorial optimization," 1997.

[27] F. Alizadeh and D. Goldfarb, "Second-order cone programming," *Mathematical Programming*, vol. 95, no. 1, pp. 3–51, Jan. 2003.

1536-1276 (c) 2021 IEEE. Personal use is permitted, but republication/redistribution requires IEEE permission. See https://www.ieee.org/publications/rights/index.html for more information.
Authorized licensed use limited to: The Ohio State University. Downloaded on March 15,2022 at 15:54:36 UTC from IEEE Xplore. Restrictions apply.

This article has been accepted for publication in IEEE Transactions on Wireless Communications. This is the author's version which has not been fully edited and content may change prior to final publication. Citation information: DOI 10.1109/TWC.2021.3125924, IEEE Transactions on Wireless Communications

[28] C. Sun and R. Dai, "An iterative rank penalty method for nonconvex quadratically constrained quadratic programs," *SIAM Journal on Control and Optimization*, vol. 57, no. 6, pp. 3749–3766, Nov. 2019.

[29] R. M. Gray, "Toeplitz and circulant matrices: A review," *Foundations and Trends® in Communications and Information Theory*, vol. 2, no. 3, pp. 155–239, Jan. 2006.

[30] Z. Zhu and M. B. Wakin, "On the asymptotic equivalence of circulant and toeplitz matrices," *IEEE Transactions on Information Theory*, vol. 63, no. 5, pp. 2975–2992, May 2017.

[31] M. S. Lobo, L. Vandenberghe, S. Boyd, and H. Lebret, "Applications of second-order cone programming," *Linear Algebra and its Applications*, vol. 284, no. 1, pp. 193 – 228, Nov. 1998, international Linear Algebra Society (ILAS) Symposium on Fast Algorithms for Control, Signals and Image Processing.

[32] B. R. Marks and G. P. Wright, "Technical note—a general inner approximation algorithm for nonconvex mathematical programs," *Operations Research*, vol. 26, no. 4, pp. 681–683, Aug. 1978.

[33] Y. Rahmatallah and S. Mohan, "Peak-to-average power ratio reduction in ofdm systems: A survey and taxonomy," *IEEE Communications Surveys Tutorials*, vol. 15, no. 4, pp. 1567–1592, Mar. 2013.

[34] S. H. Han and J. H. Lee, "An overview of peak-to-average power ratio reduction techniques for multicarrier transmission," *IEEE Wireless Communications*, vol. 12, no. 2, pp. 56–65, Apr. 2005.

[35] S. Zhang and Y. Huang, "Complex quadratic optimization and semidefinite programming," *SIAM Journal on Optimization*, vol. 16, no. 3, pp. 871–890, July 2006.

[36] G. Cui, H. Li, and M. Rangaswamy, "MIMO radar waveform design with constant modulus and similarity constraints," *IEEE Transactions on Signal Processing*, vol. 62, no. 2, pp. 343–353, Jan. 2014.

[37] G. Cui, X. Yu, G. Foglia, Y. Huang, and J. Li, "Quadratic optimization with similarity constraint for unimodular sequence synthesis," *IEEE Transactions on Signal Processing*, vol. 65, no. 18, pp. 4756–4769, June 2017.

[38] D. P. Palomar, M. A. Lagunas, A. Pascual, and A. P. Neira, "Practical implementation of jointly designed transmit receive space-time IIR filters," in *Proceedings of the Sixth International Symposium on Signal Processing and its Applications (Cat.No.01EX467)*, vol. 2, Aug. 2001, pp. 521–524 vol.2.

[39] J. Yeh, *Real analysis: theory of measure and integration*. World Scientific Publishing Company, 2006.

[40] Y.-C. Wang, J.-L. Wang, K.-C. Yi, and B. Tian, "PAPR reduction of OFDM signals with minimized EVM via semidefinite relaxation," *IEEE Transactions on Vehicular Technology*, vol. 60, no. 9, pp. 4662–4667, Sept. 2011.

[41] M. Grant and S. Boyd, "CVX: Matlab software for disciplined convex programming, version 2.1," http://cvxr.com/cvx, Mar. 2014.

[42] K. C. Toh, M. J. Todd, and R. H. Tütüncü, "SDPT3 — a matlab software package for semidefinite programming, version 1.3," *Optimization Methods and Software*, vol. 11, no. 1-4, pp. 545–581, 1999.

[43] M. K. Simon and M.-S. Alouini, *Digital communication over fading channels*. John Wiley & Sons, 2005, vol. 95.

[44] J. L. Jerez, G. A. Constantinides, and E. C. Kerrigan, "An FPGA implementation of a sparse quadratic programming solver for constrained predictive control," in *Proceedings of the 19th ACM/SIGDA International Symposium on Field Programmable Gate Arrays*, ser. FPGA '11. New York, NY, USA: ACM, Feb. 2011, pp. 209–218.

Ceyhun D. Ozkaptan (Student Member, IEEE) received the B.S. degree in electrical and electronics engineering from Bilkent University, Turkey, in 2016. He is currently pursuing the Ph.D. degree with the Department of Electrical and Computer Engineering, The Ohio State University, Columbus, OH, USA. His current research interests include wireless communications, signal processing, radar imaging, and optimization.

Eylem Ekici (Fellow, IEEE) received the B.S. and M.S. degrees in computer engineering from Bogaziçi University, Turkey, in 1997 and 1998, respectively, and the Ph.D. degree in electrical and computer engineering from the Georgia Institute of Technology, in 2002. He is currently a Professor with the Department of Electrical and Computer Engineering, The Ohio State University. His current research interests include 5G+ communication systems, vehicular communication systems, and dynamic spectrum access, with a focus on algorithm design and resource management. He was the General Co-Chair of ACM MobiCom 2012 and ACM MobiHoc 2020. He was also the TPC Co-Chair of the IEEE INFOCOM 2017. He is an Associate Editor-in-Chief of the IEEE TRANSACTIONS ON MOBILE COMPUTING, and a former Associate Editor for the IEEE/ACM TRANSACTIONS ON NETWORKING, the IEEE TRANSACTIONS ON MOBILE COMPUTING, and Computer Networks.

Onur Altintas (Member, IEEE) received the B.S. and M.S. degrees from Middle East Technical University, Ankara, Turkey, and the Ph.D. degree from the University of Tokyo, Japan, all in electrical engineering. He is currently the InfoTech Labs Fellow at InfoTech Labs, Toyota North America R&D, in Mountain View, California. He has been with the Toyota Group since 1999 in various roles in New Jersey, Tokyo, and California. He has been the co-founder and general co-chair of the IEEE Vehicular Networking Conference (IEEE VNC) since 2009. He serves in the editorial boards of IEEE Intelligent Transportation System Magazine, IEEE Transactions on Intelligent Vehicles, and IEEE Vehicular Technology Magazine. He an elected Board Member of the IEEE Vehicular Technology Society between 2016 and 2018. He was an IEEE Distinguished Lecturer between 2011-2015 and an IEEE Distinguished Speaker between 2015-2018.

1536-1276 (c) 2021 IEEE. Personal use is permitted, but republication/redistribution requires IEEE permission. See https://www.ieee.org/publications/rights/index.html for more information.
Authorized licensed use limited to: The Ohio State University. Downloaded on March 15,2022 at 15:54:36 UTC from IEEE Xplore. Restrictions apply.